Chemical composition and source identification of PM_{10} in five North Western European cities

Sarkawt M.L. Hama [1] [2], Rebecca L. Cordell [1], Jeroen Staelens [3], Dennis Mooibroek [4], and Paul S. Monks [1]

[1] Department of Chemistry, University of Leicester, Leicester LE1 7RH, UK

[2] Department of Chemistry, School of Science, University of Sulaimani, Sulaimani, Kurdistan region, Iraq

[3] Flanders Environment Agency (VMM), Department Air, Environment and Communication, Belgium

[4] National Institute of Public Health and the Environment, Centre for Environmental Quality (MIL), Department for Air and Noise Analysis (ILG), PO Box 1, 3720 BA Bilthoven, The Netherlands

Correspondence to: Paul S. Monks (psm7@le.ac.uk)

Highlights:

- A comparison study of PM_{10} chemical composition in five cities across North-West Europe.
- Clear seasonal variation of PM_{10} with higher levels in winter.
- The major components of PM_{10} are secondary inorganic aerosol, followed by organic matter and mineral dust at the urban sites.
- Secondary inorganic aerosol was found to have the largest contribution to PM_{10} in spring at the five sites.

Keywords: PM_{10}, chemical composition, seasonal variation, mass closure, PCA

Abstract

Particulate matter (PM) is a complex, heterogeneous mixture that changes in time and space. It has many different chemical constituents, several of which have been identified as potential contributors to toxicity, and varying physical characteristics. Identifying and quantifying the effects of specific components or source-related combinations on human health, particularly when particles interact with other co-pollutants, therefore represents one of the most challenging areas of environmental health research. Owing to the importance of PM_{10} chemical composition in understanding particulate pollution sources, 1942 PM_{10} samples were simultaneously collected at five sites (four urban background sites located in Amsterdam (AD), Antwerp (AP), Leicester (LE) and Lille (LL), and one industrial site at Wijk aan Zee (WZ)) across North-West Europe from April 2013 to May 2014, and chemical species and sources of PM_{10} were investigated. PM_{10} samples were chemically analysed for water-soluble ions (NO_3^-, SO_4^{2-}, Cl^-, NH_4^+, Na^+, K^+, Mg^{2+}, and Ca^{2+}), carbonaceous species (OC, and EC), minerals (Al, Ca, Fe, Ti, and K), trace elements (As, Ba, Cd, Cr, Cu, Mn, Mo, Ni, Pb, Sb, V, and Zn), and monosaccharides (levoglucosan, galactosan, and mannosan). Spatial and seasonal variations of the atmospheric concentrations of species were also investigated. In order to reconstruct the particle mass, the determined constituents were classified into seven classes as follows: mineral dust (MD), organic matter (OM), elemental carbon (EC), trace elements (TE), sea salt (SS), secondary inorganic aerosol (SIA), and monosaccharides (MSS). Strong correlations ($R^2 = 0.88-0.96$) were found between chemically determined and gravimetrically measured PM_{10} masses for all sites. According to the chemical mass closure found, the major components of PM_{10} were SIA, followed by OM and MD at the four urban sites, and the major components of PM_{10} were SIA, followed by MD and SS at an industrially influenced site. SIA dominated the PM_{10} profiles at all sites, accounting for 36, 35, 32, 36, and 32% at AD, AP, LE, LL, and WZ, respectively. Five PCA factors explained 67, 80, 76, and 74% of the variance of the data at AD, AP, LL and WZ respectively. In addition, four factors are extracted for LE site explaining 71% of the variance. The PCA results showed that secondary aerosols, biomass burning, and traffic emissions were the most important sources across north-west Europe.

1. Introduction

Although air quality in Europe has improved significantly over the past decades, air pollution is still the single largest environmental health risk in Europe with recent studies suggesting that the disease burden resulting from air pollution is significant (EEA, 2016). Ambient particulate matter (PM) is a heterogeneous mixture of organic and inorganic constituents produced from a large variety of mechanisms linked with both natural and anthropogenic sources. Numerous studies have showed that PM exposure is strongly linked with the increase risk of mortality, respiratory, and heart diseases (de Kok et al., 2006; Dockery and Stone, 2007; Heal et al., 2012; Meister et al., 2012; Pope and Dockery, 2006). PM can also impact the climate, ecosystem, and visibility by various important atmospheric processes (IPCC, 2008; Isaksen et al., 2009; Taiwo et al., 2014a).

Nowadays, most studies focus on chemical characteristics of PM and toxicological studies in an effort to find and identify the PM properties (e.g. particle number, size, surface, chemical composition) that have the most significant impact on health and environment. There is great scientific interest in the chemical composition of ambient PM, which depends on a variety of factors including the time of year, the sources of PM and the weather conditions (Röösli et al., 2001). Numerous chemical constituents of atmospheric PM, including organic compounds, heavy metals, trace elements, ions, have the potential to adversely affect human health. The European Union has established ambient air quality limits for some toxic elements, such as lead, arsenic, nickel, mercury, cadmium, and polycyclic aromatic hydrocarbons (EC, 2004).

The north-western part of Europe is considered as a hot spot zone for air pollution with high outdoor concentrations of, amongst others, particulate matter and nitrogen oxides (EEA, 2014). Particulate matter is a complex mixture resulting from several natural and anthropogenic sources including sea salt, suspended dust, pollen, volcanic ash, combustion processes, industrial activities, vehicle tyre, brake and road surface wear. Epidemiological studies attribute the most significant health impacts of air pollution to PM (WHO, 2005), although currently it is still unclear which specific properties (such as size or chemical composition) or sources of aerosol particles are most relevant to health effects (Kelly and Fussell, 2012). Ambient PM concentrations vary substantially between and within regions, as indicated by routine air quality monitoring networks. In urban areas, in addition to background PM concentrations, often imported, traffic-related emissions and domestic heating can significantly contribute to ambient PM levels (EEA, 2014).

Current monitoring efforts generally focus on the mass concentration of PM_{10} and $PM_{2.5}$ in line with current air quality legislation (2008/20/EC), but these data generally do not allow the

assessment of differing sources. To facilitate the development of health-relevant air quality policies in the north-western part of Europe a better understanding of sources and composition of PM is required. A number of studies have reported sources and composition of PM in NW Europe (AQEG, 2012; Crilley et al., 2017; Mooibroek et al., 2011; Vercauteren et al., 2011; Waked et al., 2014; Weijers et al., 2011). However, no studies to date have reported a comparative analysis of PM_{10} chemical composition at five cities across north-west Europe. In this context, the main aim of this study is to compare chemical composition, seasonal and spatial variability, chemical characteristics of ambient PM_{10} concentrations at four urban background sites, and one industrial site located in NW Europe, using a harmonized approach for aerosol sampling and laboratory analyses. Moreover, a mass closure model was applied to daily PM_{10} samples to test whether the gravimetrically determined mass can be reconstructed by the chemically determined components at the five sampling sites.

The study was carried out between April 2013 and May 2014 over which time aerosol samples were collected daily (24 hour exposure) at fixed sites in Amsterdam (AD), Antwerp (AP), Leicester (LE), Lille (LL) and Wijk aan Zee (WZ). This study was carried out as part of the JOint Air QUality INitiative (JOAQUIN, www.joaquin.eu), an INTERREG IVB NWE funded European project, aimed at supporting health-oriented air quality policies in Europe (Cordell et al., 2016; Hama et al., 2017a, 2017b, and 2017c; Hofman et al., 2016; Joaquin, 2015).

2. Experimental

2.1 Sampling sites

Aerosol samples were collected at five sites in NW Europe: Amsterdam (AD; The Netherlands), Wijk aan Zee (WZ; The Netherlands), Antwerp (AP; Belgium), Leicester (LE; United Kingdom) and Lille (LL; France) (see Figure 1). The detailed site descriptions are summarised in Table 1. Site WZ is an industrial monitoring site about 30 km from Amsterdam. The four other sites are considered to be urban background sites for PM_{10} monitoring. Details about the characteristics and locations of the sampling sites can be found in Cordell et al. (2016). For a detailed overview of the sampling sites and the JOAQUIN project, the reader is referred to the final report (Joaquin, 2015).

2.2 PM_{10} sampling

Sampling was carried out for 14 months (426 days) from 1 April 2013 to 31 May 2014, except for LL where the measurements started 2 months later (5 June 2013 to 31 May 2014). The collected number of filters for each monitoring sites are summarised in Table S1. The samples were collected daily (24 hour exposure) onto 47 mm quartz filters (Pall Tissuquartz^{TM} filters, 2500 QAT-UP) using a sequential sampler (Derenda PNS16 at AD and WZ and Leckel SEQ47/50 at AP, LE and LL) with a PM_{10} inlet running at 2.3 m^3 h^{-1} for 24 h per filter. Filter samples collected every 6th day for the period were analysed for water-soluble ions, elemental and organic carbon, metals, and monosaccharide anhydrides. Flows were checked every 14 days when changing the filter compartments. Filters were weighed before and after sampling in order to determine total PM_{10} collection. For pre- and post-sampling weighing filters were conditioned at $20 \pm 1°C$ and $50 \pm 5\%$ relative humidity for 48 h, weighed, left for a further 24 h and re-weighed. Both the real samples and the blank filters were weighed and the PM_{10} mass for the actual samples were corrected for the net masses obtained from the blank filters.

2.3 Chemical analysis

After gravimetric analysis, all filters (blanks and exposed) were stored at -18°C. From the filters for chemical analysis, six punches of 1 cm^2 were taken. Identical 1.0 cm x 1.0 cm punches (SunSet Laboratory Inc., USA) were used. If the planned filter (every 6th) day was not available for a site, the filter of the preceding or following day was used for that site only. Three punches were subjected to analyse water soluble ions, one punch was subjected to determine respectively the elemental composition, elemental and organic carbon (EC/OC) and monosaccharide anhydrides, The method detection limits (MDLs) values ($\mu g/m^3$) were as follows: 0.01 (EC and OC), 0.014 (NO^{3-}), 0.004 (Cl^-), 0.007 (SO_4^{2-}), 0.007 (Na^+), 0.007 ($NH4^+$), 0.007 (K^+), 0.007 (Mg^{2+}), and 0.014 (Ca^{2+}). The MDLs (ng/m^3) for elements were, 0.21 (Mn, Pb, Sb, and V); 0.53 (As, Ni, Ti and Ba); 0.11 (Cd, and Mo); 1.1 (Cr, and Cu). The MDLs ($\mu g/m^3$) for Levoglucosan (Lev), mannosan (Man) and galactosan (Gal) were equal, 0.11. The median values of the results of the field blank filters were used to apply a blank correction for the results of the monosaccharide anhydrides, water-soluble ions, and elements of the exposed filters. No correction was carried out for the PM_{10} mass and EC/OC results, in line with the current air quality guidelines (EN 12341:2014 for the PM_{10} mass and technical report CEN/TR 16243 for OC).

Potassium (K^+), calcium (Ca^{2+}), magnesium (Mg^{2+}), and sodium (Na^+) were analysed by inductively coupled plasma optical emission spectroscopy (ICP-OES), and ammonium (NH_4^+), chloride (Cl^-), nitrate (NO_3^-) and sulphate (SO_4^{2-}) were analysed using ion chromatography with conductivity detection (IC-CD) (eluents: methane sulfonic acid (MSA) for NH_4^+ and NaOH for the anions). The EC/OC analysis was performed according to Technical Report CEN/TR16243 "Ambient air quality - guide for the measurement of elemental carbon (EC) and organic carbon (OC) deposited on filters". The analysis was done with a laboratory organic/elemental carbon aerosol analyser (Sunset Laboratory Inc, Tigard (OR), USA). The NIOSH protocol, which is most suitable for the traffic influenced PM_{10} samples of the Joaquin project, was selected for the analysis. Calcium (Ca), iron (Fe), potassium (K) and zinc (Zn) were analysed by ICP-OES. Aluminium (Al), titanium (Ti), vanadium (V), chromium (Cr), manganese (Mn), nickel (Ni), copper (Cu), arsenic (As), molybdenum (Mo), cadmium (Cd), antimony (Sb), barium (Ba) and lead (Pb) were analysed by inductively coupled plasma mass spectrometry (ICP-MS). Lev, Man and Gal were quantified using a validated gas chromatography-mass spectrometry (GC-MS) method described in detail by Cordell et al. (2014). An improved gas chromatography-mass spectrometry method to quantify atmospheric levels of monosaccharides (MAs) was developed and, for the first-time, fully validated. The method used an optimised, low-volume methanol extraction, derivatisation by trimethylsilylation and analysis with high-throughput GC-MS. More information about quality control and assurance (QC/QA) can be found in (Cordell et al., 2016; Joaquin, 2015; Cordell et al., 2014).

2.4 The coefficients of divergence

The correlation coefficient is a standard method used to indicate the relationship between two data sets/variables. Spearman rank correlation coefficients (r) were used to find the spatial variability between sampling sites. To evaluate intra-urban spatial variation coefficients of divergence (COD) were used (Contini et al., 2012a; Jeong et al., 2010; Krudysz et al., 2009; Turner and Allen, 2008; Wilson et al., 2005):

$$COD_{ab} = \sqrt{\frac{1}{n}\sum_{i=1}^{n}\left[\frac{(C_{ia} - C_{ib})}{(C_{ia} + C_{ib})}\right]^2} \qquad (1)$$

where C_{ia} and C_{ib} are PM_{10} concentrations in day i at sites a and b, respectively, and n is the number of observations (Krudysz et al., 2009; Wongphatarakul et al., 1998).

The COD provided information about the degree of uniformity between sampling sites. A COD value equal to zero means the concentrations are nearly identical at both sites while a value of one shows concentrations are highly different. COD values greater than about 0.20 show somewhat heterogeneous spatial distributions (Cesari et al., 2016a; Pinto et al., 2004; Wilson et al., 2005).

2.5 Reconstruction of PM_{10}

In order to understand the contributions of each constituent in PM_{10}, PM_{10} at the four urban areas and one industrial site were reconstructed by chemical mass closure. The chemical components were divided into seven categories: mineral dust (MD), organic matter (OM), elemental carbon (EC), trace elements (TE), sea salt (SS), secondary inorganic aerosol (SIA), and monosaccharides (MSS). MD is the sum of Al, Ca, Fe, and Ti multiplied by various factors (Eq. 2) to convert them to their common oxides (Al_2O_3, MgO, K_2O, CaO, Fe_2O_3, TiO_2) (Nava et al., 2012; Rodriguez et al., 2004; Terzi et al., 2010):

$$MD = 2.2\,Al + 1.16\,Mg + 0.6\,Fe + 1.63\,Ca + 2.42\,Fe + 1.94\,Ti \qquad (2)$$

As Fe can be derived from both mineral and industrial sources, in equation (2) the source of Fe is considered as mineral dust. More detail regarding the differing sources of Fe is discussed in section 3.2.3. The chemical structure of OM in the ambient PM is rather complex. When reconstructing OM, it is generally expressed as a certain factor multiplied by the measured concentrations of OC. Previous studies have suggested 1.4 is a suitable factor for organic aerosol in urban area (Harrison et al., 2003; Turpin and Lim, 2001; Vecchi et al., 2008; Viana et al., 2007) and that value is used in this work. EC is measured by direct measurements. TE (As, Ba, Cd, Cr, Cu, Mn, Mo, Ni, Pb, Sb, V, and Zn) were also added to the analysis. TE represent a small percentage of the PM_{10} total mass concentrations, however, they have a significant impact on health (McNeilly et al., 2004; Moreno et al., 2004) and environment owing to their toxicity and anthropogenic origin (Rees et al., 2004). The marine contribution was found, assuming that soluble Na^+ in PM_{10} aerosol samples comes solely from sea salt, the SS was calculated (Eq. 3) by sum of Na^+ concentrations and fractions of the concentrations

231   other water soluble ions (Cl⁻, Mg^{2+}, K^+, Ca^{2+}, SO4²⁻) based on a standard sea water composition

232   (Seinfeld and Pandis, 2006).

233

234    $$SS = [Na^+] + [ssCl^-] + [ssMg^{2+}] + [ssK^+] + [ssCa^{2+}] + [ssSO_4^{2-}] \qquad (3)$$

235

236   where ss-Cl⁻ is calculated as total $[Na^+]$ multiplied by 1.8, ss-Mg^{2+} as total $[Na^+]$ multiplied by

237   0.12, ss-K^+ as total $[Na^+]$ multiplied by 0.036, ss-Ca^{2+} as total $[Na^+]$ multiplied by 0.038, and

238   ssSO₄²⁻ as total $[Na^+]$ multiplied by 0.252. SIA was calculated as the sum of concentrations of

239   nss-SO₄²⁻ (non-sea salt, obtaining by subtracting ss-SO₄²⁻ from total concentration of SO₄²⁻),

240   NO₃⁻, and NH₄⁺ (Terzi et al., 2010). Finally, MSS is obtained by sum of the monosaccharides

241   (Lev, Gal, and Man). MSS only presents a small percentage of the PM_{10} mass but were added

242   to the analysis owing to their importance as biomass burning markers (Cordell et al., 2016;

243   Fuller et al., 2014).

244

245   ## 2.6 Principal component analysis

246   Principal component analysis (PCA) has widely been used as a statistical factor analysis

247   method capable of identifying and separating chemical components of PM according to their

248   sources in urban areas (Ciaparra et al., 2009; Cusack et al., 2013; Lawrence et al., 2013; Mari

249   et al., 2010; Shi et al., 2011). PCA was undertaken using the software XLSTAT 2016. The

250   orthogonal transformation method with varimax rotation was employed, retaining principal

251   components with eigenvalues greater than one. The PCA method can be used to factorise the

252   input data of different concentration of species assuming a linear relationship between total PM

253   mass and the component concentrations of various species (Bongiovanni et al., 2000; Hopke,

254   2000). The multivariate mathematical approach contains several steps to group the elemental

255   data. In the first step, the concentrations of species are standardised:

256

257    $$Z_{ij} = \frac{C_{ij} - C_i}{\sigma_i} \qquad (4)$$

258

259   where C_{ij} is the concentration of the variable i in the sample j, and C_i and σ_i are the mean and

260   standard deviation of the variable i for all samples involved in the method analyses. The PCA

261   model is expressed as:

262

263
$$Z_{ij} = \sum_{j=1}^{N} L_{ij} S_{js} + E_{is} \qquad (5)$$

264

265 where L_{ij} is the factor loading of the variable i in the source j with n number of sources, S_{js} is

266 the factor score of the source j for sample s and E_{is} is the residual of variable i in the sample s

267 which not accounted by j sources (factors). In this statistical analysis a set of multiple inter-

268 correlated variables is substituted by smaller independent variables by orthogonal

269 transformations. A varimax normalized rotation is applied to maximize (or minimize) the

270 values of the factor loadings of each species measured in relation to each rotated principal

271 component.

272

273

274 ## 3. Results and Discussion

275 ### 3.1 PM_{10} Mass concentrations and spatial comparison

276 Monthly variations of PM_{10} mass concentrations at the five sites are shown in Figure 2. Clear

277 seasonal variations of PM_{10} concentrations are observed at all the sampling sites throughout

278 the year. It should be noted that the observed seasonal pattern of PM_{10} at each sampling site

279 shows a high level of similarity (Figure 2) indicative of a regional characteristic for PM_{10} in

280 the north-west Europe region. The data were split into three time periods for analysis: the cold

281 period (November to April), the warm period (May to October), and the entire year. The

282 arithmetic mean and standard deviation of PM_{10} for the samples collected at the five locations

283 are given in (Table 2). High concentrations of PM_{10} in the cold period are probably attributable

284 to the higher frequency of temperature inversion and the relatively stable atmospheric

285 conditions which are not conductive to the dilution or advection of air pollutants, as well as the

286 impacts of reduced mixing height along with increased energy-based emissions including wood

287 burning (Cordell et al., 2016). Lower concentrations of PM_{10} in summer might be linked to

288 higher mixing layer heights, and reduced (heating) emissions.

289 For the experimental period (June 2013-May 2014), the PM_{10} concentrations vary from 16.1 to

290 25.6 $\mu g\ m^{-3}$ at all sites. Highest annual average concentrations of PM_{10} were measured in AP

291 (24.9 $\mu g\ m^{-3}$), and WZ (25.6 $\mu g\ m^{-3}$), which might be related to industrial activates near these

292 sites. The lowest PM_{10} levels were observed in LE (16.2 $\mu g\ m^{-3}$). The annual mean

293 concentrations were 20.7 and 22.4 $\mu g\ m^{-3}$ in AD and LL, respectively (Table 2). The number

294   of exceedances of the EU day limit value for PM_{10} (50 µg m^{-3}) was highest at AP (20 days/year)

295   and WZ (16), moderate at LL (12) and lowest at AD (8) and LE (6). Exceedances of the day

296   limit value mainly occurred in March and April. To address the spatial distribution of PM_{10} the

297   COD values have been calculated between all sites and is shown in Table 3. According to

298   previous studies (Cesari et al., 2016a; Contini et al., 2012a; Wilson et al., 2005), the threshold

299   value was set to 0.2 for the comparison of COD values of PM_{10} between all sites. Most COD

300   values were higher than this threshold, except for the site pairs AD - AP (COD = 0.162;Table

301   3, AD - WZ (0.192), and AP - LL (0.155), indicating those sites had more similar regional

302   PM_{10} pollution characteristics.

303

3.2 Characteristic of chemical species in PM_{10}

3.2.1 The water soluble ions (WSIs) analysis

306   The annual, cold period and warm period concentrations of WSIs (NO_3^-, SO_4^{2-}, Cl^-, NH_4^+, Na^+,

307   K^+, Mg^{2+}, and Ca^{2+}) for the five sites are given in Table S2. At all sites the major contributor

308   to anions was NO_3^- followed by SO_4^{2-} while the dominant cations were NH_4^+, and Na^+. In this

309   study, secondary ions NO_3^-, SO_4^{2-}, and NH_4^+ were the major WSIs in PM_{10}, which accounted

310   for 37, 35, 33, 37, and 33% of the PM_{10} concentrations (Table S3) and 79, 82, 72, 82, and 69%

311   of the total WSIs in PM_{10} for the sites AD, AP, LE, LL, and WZ, respectively. On the contrary,

312   the concentrations of primary ions such as Cl^-, Na^+, K^+, Mg^{2+}, and Ca^{2+} were relatively low,

313   which indicated that the secondary particles were the main pollutants in this region. In terms

314   of annual concentrations, the three major secondary ions in all sites followed the order of NO_3^-

315   > SO_4^{2-} > NH_4^+. Similar seasonal variations of the WSIs were observed at all sites, showing

316   higher levels in the cold period (except for SO_4^{2-}) and lower concentrations in the warm period

317   (Table S3). These patterns can be ascribed to increased domestic heating in winter (Cordell et

318   al., 2016), leading to high concentrations of precursors, the meteorological conditions as well

319   as regional transportation and secondary reactions. In addition, the higher concentrations of

320   NO_3^- and Cl^- in the cold season could be due to traffic primary emissions and biomass burning.

321   The autumn and early winter are the seasons with the most storms at sea, generating and

322   transporting sea salt to the continent. Furthermore, there might be an influence of road salting

323   during the winter. These two components react with NH_4^+ to form ammonium salt, and these

324   salts can dissociate to gaseous compounds in the warm period caused to decrease

325   concentrations of NO_3^- and Cl^- in summer. Because of higher storm activity there might be

326 more fresh sea salt during winter compared to the summer. However, relatively higher
327 concentrations of SO_4^{2-} were found during the warm period at AD, AP, and LE sites (Table
328 S3), indicating photochemical formation of sulphates at these sites (Hama et al., 2017a, and
329 2017b; Hofman et al., 2016). In addition, regional transport of ammonium sulphate from other
330 areas might be another reason. Note that the concentrations of Cl^-, Na^+, and Mg^{2+} were clearly
331 higher in WZ than at the other sites, owing to its close proximity to the North Sea. NO_3^-
332 concentrations at LE site were significantly lower than at the other sites, likely due to the fact
333 that LE site is situated in more residential area, with less traffic and lower industrial/agricultural
334 emissions. High seasonal variation was also observed for K^+ with higher levels in the cold
335 seasons, suggesting impact of biomass combustion sources in this region (Cordell et al., 2016).
336 It is interesting to note that the ratio of NO_3^-/PM_{10} was high in the cold period and low in the
337 warm period, while the SO_4^{2-}/ PM_{10} ratio was high in summer and low in the cold season
338 consistently for the five sites (Table 4). This might be linked to relatively high levels of OH
339 and O_3, high temperature and solar radiation in summer months, which are conducive for the
340 decomposition of NO_3^- and generation of SO_4^{2-} from SO_2. Additionally, the ratio SO_4^{2-}/ NO_3^-
341 in warm months is significantly higher than in other months (Table 4), which is probably
342 attributable to the dissociation of nitrate in PM_{10}. WSIs concentrations in this region are
343 comparable to those previously found in other urban sites in Europe and Asia (Takahashi et al.,
344 2008; Terzi et al., 2010; Viana et al., 2007).
345 The correlation between the WSIs during different seasons is shown in Figure S1. The
346 correlation between NO_3^- and NH_4^+ are r=0.91-0.98 (in winter), and 0.78-0.93 (in summer).
347 The correlation between SO_4^{2-} and NH_4^+ (r=0.78-0.98, in winter) shows a similar tendency with
348 that between NO_3^- and NH_4^+ during different seasons at all sampling sites (Figure S1),
349 indicating the secondary origin. Higher correlations between NO_3^- and NH_4^+ and between SO_4^{2-}
350 and NH_4^+ were observed at all monitoring sites. However, lower correlations were found
351 between NH_4^+ and Cl^-, suggesting that NH_4^+ (coming from ammonia mainly emitted by
352 farming) could be major source of ammonium nitrate, ammonium sulphate, and ammonium
353 hydrogen sulphate in these cities (Figure S1). In addition, the correlation between Cl^- and Na^+,
354 and Cl^- and Mg^{2+} was significant across seasons and sampling sites. This observation could be
355 related to the presence of marine aerosol and crustal matter for Mg^{2+}.
356
357
358
359

3.2.2 Carbonaceous material analysis

The mean concentrations of OC, EC for the annual, cold, and warm periods are given in Table S3. The annual average concentrations of OC and EC are 3.02, and 0.58 $\mu g\,m^{-3}$, accounting for 12.7%, and 2.5% of PM_{10} (AD site), 4.40, and 1.56 $\mu g\,m^{-3}$, accounting for 14.43%, and 5.12% of PM_{10} (AP site), 3.39, and 0.95 $\mu g\,m^{-3}$, accounting for 17.54%, and 4.94% of PM_{10} (LE site), 4.47, and 1.19 $\mu g\,m^{-3}$, accounting for 15.0%, and 3.99% of PM_{10} (LL site), 2.81, and 0.81 $\mu g\,m^{-3}$, accounting for 9.68%, and 2.79% of PM_{10} (WZ site) (see Table S4). The concentrations of OC and EC are higher in the cold period and lower in the warm months. The mean OC concentration was highest in AP and LL, and lowest in WZ. The average EC concentration was highest in AP, followed by LL, and lowest in AD (Table S4). Total carbonaceous aerosol (TCA) was calculated by summing EC and OM (multiplying the concentrations of OC by 1.4) (Turpin and Lim, 2001). The annual levels of TCA are 4.8 $\mu g\,m^{-3}$ (20.4% of PM_{10}), 7.7 $\mu g\,m^{-3}$ (25.3% of PM_{10}), 5.7 $\mu g\,m^{-3}$ (30% of PM_{10}), 7.5 $\mu g\,m^{-3}$ (25.0% of PM_{10}), and 4.8 $\mu g\,m^{-3}$ (16.4% of PM_{10}) at AD, AP, LE, LL, and WZ sites, respectively (Table S4). Several studies state that the ratios of OC/EC from biomass burning and coal combustion are relatively higher, while that of traffic emissions are relatively lower (Safai et al., 2014; Schauer et al., 2002). The concentration ratio of OC/EC can be used to identify primary and secondary aerosol sources. EC is a component that is related to the combustion of fossil fuels and of (diesel) traffic in particular (primary aerosol sources), while OC exists in both primary and secondary organic aerosol (SOA) sources produced in complex photochemical reactions (Chen et al., 2016; Gray and Cass, 1986; Ho et al., 2002). The highest annual ratio of OC/EC was observed in AD (5.15), while lowest value was found in AP (2.81) (Table S4), as a result of moderate secondary organic carbon combined with low EC levels compared to the other sites. The ratio of OC/EC have been found in the range 1-4 in the previous studies for PM_{10} at urban sites (Wang et al., 2005, and references therein).

If the ratio of OC/EC is greater than 2.0, it can be considered that OC is contributed by both primary and secondary sources, and a higher ratio indicates a higher contribution of SOA (Cao et al., 2009). In this paper, the OC/EC ratios at the five sites were in the range of 2.81-5.15, showing a clear prevalence of organic carbonaceous species over EC which indicates potential SOA formation.

The scatter plots of OC and EC concentrations at the five sites are shown in Figure 3. The correlations between the OC and EC were stronger in cold months (winter and autumn) at the AP, LE, LL, and WZ sites (R^2 = 0.52-0.87 (Figure 3), r = 0.61-0.93 (Figure S2), suggesting

393   that OC and EC might be influenced by the same sources to some extent in the cold period at

394   these sites. However, the correlations between OC and EC were relatively weaker at the AD

395   site ($R^2 = 0.12$ (Figure 3), r = 0.34-0.41 (Figure S2)). Furthermore, very weak correlations (R^2

396   = 0.07-0.3 (Figure 3), r = 0.08-0.55 (Figure S2)) were observed during the warm period,

397   especially in summer at the five sites. This might be associated to the OC and EC were affected

398   by different emission sources at the sampling sites in summer.

399

400

401   **3.2.3 Minerals and trace elements analysis**

402   The average concentrations (annual, cold, and warm periods) of the seventeen detected

403   elements (Al, As, Ba, Ca, Cd, Cr, Cu, Fe, K, Mn, Mo, Ni, Pb, Sb, Ti, V, and Zn) in PM_{10} have

404   been quantified at the five sampling sites (Table S5). The annual percentages of total detected

405   minerals (excluding K) in PM_{10} were 4.5, 6.1, 5.3, 6.0, and 9.1% at AD, AP, LE, LL, and WZ,

406   respectively. The average levels of the various elements are highly differentiated. Crustal

407   elements (Al, Ba, Ca, Fe, Mn, and Ti) dominate the identified elements of PM_{10}, accounting

408   for 91.3, 90.8, 91.7, 92.2%, and 94.5% of the total detected minerals at AD, AP, LE, LL, and

409   WZ, respectively. The concentrations of the crustal metals were higher during the cold period

410   and lower in the warm period (Table S5), which was consistent with the seasonal variation of

411   PM_{10} mass concentration. Different pattern for the crustal has been found in southern Europe

412   which was the crustal fraction with contributions in winter and spring lower than those in

413   summer and autumn. This might be related to limited rain and dry soil in spring and summer

414   could favour dust resuspension (Cesari et al., 2018; Querol et al., 2008). In addition, trace

415   elements (As, Ba, Cd, Cr, Cu, Mo, Ni, Pb, Sb, V and Zn) accounted for 8.7, 9.2, 8.3, 7.8, and

416   5.5% of the total detected minerals at AD, AP, LE, LL, and WZ, respectively. The levels of the

417   trace elements were relatively higher at AD, AP, and LE sites, suggesting higher influence of

418   traffic emissions and re-suspended soil. Trace elements and metals the sub-micron size range

419   may arise from tire wear, abrasion of brakes, and re-suspension of road dust, as well as from

420   lubricating oil additives and engine wear debris accumulated in the oil (Gustafsson et al., 2008;

421   Saffari et al., 2013). To show the impacts of anthropogenic emissions on the concentrations of

422   particle associated elements, an enrichment factor (EF) analysis has been employed in previous

423   studies (Adamo et al., 2011; Almeida et al., 2017; Kim et al., 2002; Liu et al., 2017; Samiksha

424   et al., 2017).

425   In this work, Al was used as a reference element (Lin et al., 2015; Samiksha et al., 2017). The

426   EF was calculated as:

427

428   $$EF_X = \frac{(C_X|C_R)\text{aerosol}}{(C_X|C_R)\text{crust}} \qquad\qquad (6)$$

429

430   where C_X and C_R are the concentrations of the focus and reference element in the aerosol and

431   upper continental crust, respectively (Wedepohl, 1995). The EF analysis provides only

432   qualitative information, owing to the wide variation of the elemental concentrations of the

433   upper crust at various locations. The EF was not carried out for K as almost all of the samples

434   were below the limits of detection. The EF values of the elements in PM_{10} at the five sampling

435   sites are shown in Figure 4. The EF values for Fe, Mn, Ti, Ba, and Ca were all close to 10 at

436   the sampling sites (except WZ), suggesting that these elements are mostly derived from the

437   crustal sources. It should be noted that the EF values for Fe (EF = 20.3), and Mn (EF = 37.0)

438   at WZ site were higher than the other sites, indicating that these elements were mainly from

439   industrial activities such as the major steel industry in this area.   The EF values for V, Cr, at

440   all sampling sits, and Fe and Mn at the WZ site were in the range of 10-100, suggesting both

441   natural and anthropogenic sources (such as traffic emissions and industry). Of the other

442   elements, PM_{10} was highly enriched (EF>100) in As, Cd, Cu, Mo, Ni, Pb, Sn, and Zn at all

443   sampling sites, indicating that these elements are related with human activities, such as

444   vehicular traffic, industrial sources and so on. Notably, amongst all elements in PM_{10} at all

445   sites, Cd and Sb were highly enriched. Cd was highest at AP and WZ, followed by LL. For AP

446   this is likely due to industrial activities at Umicore (Hoboken) and for WZ likely due to Tata

447   Steel. In addition, previous studies have suggested that the high EF values of Sb, Zn, and Cu

448   might be related to brake wear (Amato et al., 2016). Mechanical abrasion of brake wear and

449   tires are possible sources of Cu, Zn, and S accounting for their higher enrichment in PM_{10}

450   (Amato et al., 2009). The enriched minerals in PM_{10}, particularly Sb, Cu, and Zn, are known

451   to be used in some materials, such as additives to vehicle lubricants as anti-oxidants and anti-

452   corrosives and in in brake linings (Thorpe and Harrison, 2008). Finally, it can be concluded

453   that the anthropogenic sources (vehicular traffic emissions, industrial activities, and brake

454   wear) all contribute to the abundance of these elements.

455

456

457

3.2.4 Monosaccharide anhydrides (MAs) analysis

Monosaccharide anhydrides (MAs) such as levoglucosan (Lev), Mannosan (Man) and Galactosan (Gal) have been considered as candidate tracers for residential wood combustion (Simoneit et al., 1999). Lev, Man, and Gal were detected in all PM_{10} aerosol samples at the sampling sites. The annual atmospheric concentrations of Lev, Man, and Gal were 49.9, 12.59, and 4.41 ng m^{-3}, 99.69, 26.55, and 12.03 ng m^{-3}, 52.83, 16.01, and 5.93 ng m^{-3}, 157.7, 35.39, and 12.97 ng m^{-3}, 33.5, 10.01, and 5.08 ng m^{-3} at AD, AP, LE, LL, and WZ, respectively, details are given in Table S6. The concentrations of MAs in the cold period were on average 5.05, 3.52, 3.49, 7.27, and 4.95 times higher than those in the warm period for AD, AP, LE, LL, and WZ, respectively. The MAs (particularly Lev) concentrations at LL were clearly higher than at the other sites, indicating more biomass/wood burning in LL compared to other regions in the study (Waked et al., 2014). The seasonal variation of MAs (high levels in the cold period, low in summer) can be related to the impact of increased biomass burning from residential heating in winter, and also may be linked to different meteorological condition (wind speed, temperature, and mixing layer height) in cold and warm periods in the north-west European area. Additionally, low concentrations of MAs (especially Lev) or degradation of Lev in summer may be linked to present high OH radicals in atmosphere (Hoffman et al., 2010). However, whilst this might have significant effects in tropical regions it is likely to have little impact in NW Europe (Cordell et al., 2016). Lev, used as a marker of biomass combustion and was the most abundant MA measured during all periods in this study, while Gal was found in the lowest concentrations in all seasons (Table S6). The correlation between the MAs and PM_{10} are shown in Figure S3. The highest correlation (r=0.77-0.89, see Figure S3) between the MAs and PM_{10} concentrations were observed in the cold period at all sampling sites, suggesting a greater contributions of MAs (particularly Lev) to PM_{10} in this period. Low and even negative correlations (r= -0.33-0.41, see Figure S3) were found in summer, indicating that PM_{10} mass was influenced by other sources than biomass burning in summer. The similar correlation can be found between the Lev and the other MAs (Man and Gal) which are high in the cold period and low in the summer (see Figure S3). More information about MAs in this region can be found in a recent study (Cordell et al., 2016).

3.3 Chemical Mass closure of PM_{10}

The results of the chemical mass closure (CMC) for PM_{10} at the five sites are shown in Table 5 and Figure 5. For the purpose of chemical mass closure the chemical components of PM_{10} were divided into seven classes as discussed in section 2.5. The relative contributions reflect differences in processes and emission sources governing PM_{10} aerosol composition (Putaud et al., 2004). MD, OM, SS, and SIA were the main contributors to PM_{10} mass concentrations at all sites. SIA dominated the PM_{10} profiles at all sites, accounting for 35.9, 34.5, 32.3, 36.4, and 31.6% at AD, AP, LE, LL, and WZ, respectively (see Figure 5). Organic matter was also a major components of PM_{10} at all sites (except WZ), accounting for 17.8, 20.2, 24.6, 21.0, and 13.5% for AD, AP, LE, LL, and WZ sites, respectively (Figure 5). High contributions of mineral dust were also found in AP and WZ, accounting for 12.4 and 19.2%, respectively. This contribution may be attributed to emissions from industrial activities at these sites. Notably, sea salt constituted a significant fraction of PM_{10} at LE, and WZ, accounting for 15.14 and 15.7%, respectively (see Figure 5). This might be linked to the photochemical formation of sulphates at LE as shown in previous studies (Hama et al., 2017a, and 2017b; Hofman et al., 2016), and owing to the close distance to the North Sea (for WZ site). Furthermore, unknown fractions were also observed at all sites (see Figure 5). UNK is generally attributed to the water content of PM which is related with the estimation of the composition of crustal minerals and organic matter (Tsyro, 2005).

The average concentrations of main contributors (SS, and SIA) to PM_{10} are higher in the cold period and lower in the warm period (Table 5), which is consistent with the PM_{10} seasonal pattern. However, there are different seasonal contributions to PM_{10} at between the sites. For example, higher percentages of MD in PM_{10} were observed in winter and autumn at AD, LE, LL, and WZ sites (see Figure 5). In the case of organic matter, OM was higher in the winter at all sites, and relatively lower in the warm period (see Table 5). EC is mostly emitted as primary soot from combustion sources; therefore it has higher levels in the cold period (winter and autumn) and lower levels in summer at all sites (Figure 5). This could be related to the thermal inversion, lower development of the mixing layer concentrates the EC emitted by diesel cars and other combustion sources (such as wood burning during cold period) across north-west Europe. Moreover, SS showed a higher contribution to PM_{10} in winter and autumn months at all sites (see Figure 5). This is consistent with a previous study (Alastuey et al., 2016). The average concentrations of SS in the cold period is relatively higher at LE (28%), and WZ (23%) than at the other monitoring sites. Higher percentage of SS at LE site can be associated to the

525 passage of clean continental marine air through the monitoring site (Taiwo et al., 2014c).

526 Neutralisation of hydrochloric acid (HCl) vapour (produced form incinerator and power plants)

527 by ammonia may also be responsible for chloride formation in PM_{10} (Harrison and Yin, 2000).

528 Furthermore, SIA showed a higher percentage contribution in the spring, and a lower one in

529 summer (see Figure 5). A combination of meteorological conditions and various emission

530 sources led to highly elevated SIA concentrations in this region in spring, mainly due to high

531 ammonium nitrate concentrations. This is likely related to increased emissions of NH_3 when

532 manure is spread on agricultural lands, and the subsequent increase in the formation of

533 NH_4NO_3.In addition, the high contribution by SIA at LE site is a reflection of the east to west

534 gradient in secondary nitrate and sulphate found all over the United Kingdom (AQEG, 2012;

535 Taiwo et al., 2014b). Finally, the correlation between gravimetric and calculated PM_{10} mass

536 are shown in Figure 6. It can be seen that there is a strong correlation between gravimetric and

537 chemically determined PM_{10} mass at all the sampling sites (R^2=0.88-0.96, see Figure 6). This

538 result supports the validity of the mass closure approach with the measured species accounting

539 for the majority of PM_{10} mass.

540

3.4 Identification of emission source by PCA

542 The principal component analysis (PCA) builds on the variability of the PM components at the

543 receptor site and tends to identify species that have a similar correlation in time and space and

544 combines these species. The combination of these species can be used to link them to known

545 sources. In this statistical method a set of multiple inter-correlated variables is replaced by

546 smaller independent variables by orthogonal transformations. A varimax normalized rotation

547 was applied to maximize/minimize the values of the factor loadings of each species measured

548 in relation to each rotated principal component. The eigenvalue for extracted factors was more

549 than 1.0. The number of factors was detected so that they explain the highest maximum total

550 variance of the data. In the literature, it is recommended to use 50–200 samples subject to

551 variable ratios (STV) of 3–20 (de Winter et al., 2009). In this study, statistical analyses are

552 obtained using XLSTAT 2017. Factor analysis was applied to a population with the following

553 data: N = minimum 93, p= 29 and STV >3.2. The considered components (p) were: Al, As,

554 Ba, Cd, Fe, Cr, Cu, Fe, Mn, Mo, Ni, Pb, Sb, Ti, V, Zn, Cl^-, NO_3^-, SO_4^{2-}, Na^+, NH_4^+, K^+,

555 Mg^{2+}, Ca^{2+}, OC, EC, Gal, Man, and Lev.

556 Five factors were extracted as principal components (eigenvalue >1) that explained 67.1,

557 80.2, 76.2, and 73.3% of the variance of the data at AD, AP, LL and WZ respectively. In

558   addition, four factors were extracted for LE site explaining 71.1% of the variance (Table 6).

559   The first factor (PC1) is responsible for 10.7, 14.2, 22.4 12.6 and 16.1% of the total variance

560   at AD, AP, LL, WZ and LE, respectively. PC1 is designated as crustal origin by the observation

561   of the major contribution of Ca^{2+}, Ba, Zn and Ti. LL site had a greater dispersion of the

562   variables, in fact the first principal component was influenced by anthropogenic elements, such

563   as As, Cd, Cr, Cu; thus describing a possible industrial emission contribution (Querol et al.,

564   2007). The second factor (PC2) is responsible for 13.2, 14.6, 18.1, 12.6, and 12.9% of the total

565   variance at AD, AP, LL, WZ and LE, respectively. PC2 is loaded with NH_4^+, NO_3^-, SO_4^{2-} and

566   to a smaller extent V(Contini et al., 2010); it represents secondary inorganic aerosol (SIA)

567   (Hama et al., 2017b; Hofman et al., 2016). The presence of V in PC2 could indicate a

568   contribution of anthropogenic emissions (possible sources of V and SO_2). These sources are

569   likely linked to emissions from ships (for both AD and AP sites) and the emissions from power

570   plants, located in the large industrial areas (AD, AP, and LL sites). The third factor (PC3) is

571   responsible for 11.9, 10.9, 11.4, 12.6, and 11.2% of the total variance at AD, AP, LL, WZ and

572   LE, respectively. PC3 is characterized by Na^+ and Cl^- and K^+ for AP, LL, WZ and LE, while

573   for AD site, Na^+ and Cl^- was correlated with Mg^{2+}. All the previous components were identified

574   as part of marine aerosol (see Table 6). The fourth component (PC4) is responsible for 21.6,

575   12.9, 16.9, 16.3, and 31.1% of the total variance at AD, AP, LL, WZ and LE, respectively. The

576   source is associated with biomass burning. In AD, LL, WZ and LE sites the source is

577   characterized by Lev, Man, and Gal. Furthermore, in AD and LE the sites, the presence of

578   metals (i.e. As, Cd, and Pb) associated with K^+ and OC (Bernardoni et al., 2011) confirms even

579   more the hypothesis of biomass burning (Cordell et al., 2016), most likely, from power plants

580   (Maenhaut et al., 2016). However, at the LE site the source is also influenced by vehicle

581   emissions (i.e. EC, Cu, Cr, Mo and Sb) (Table 6). The fifth component (PC5) is responsible

582   for 10.6, 27.7, 7.5, and 20.5% of the total variance in AD, AP, LL, WZ sites, respectively. AD

583   site is influenced by Cu, Ni, and V. Furthermore, V/Ni ratio is approximately 0.6; this ratio is

584   associated to diesel fuel combustion (Cesari et al., 2014), confirming the hypothesis of the

585   association with petrol combustion and traffic emissions. AP site is characterized by EC, Al,

586   Cu, Cr, As, Mo, and to a minor extent Cd, Mn, Pb and OC. These elements highlight many

587   anthropogenic sources, in particular metal industries and vehicle emissions (diesel combustion

588   and brakes). LL site is characterized by the presence of Cu and Sb, usually used brake pads

589   wears (Furuta et al., 2005; Muránszky et al., 2011). In addition, also WZ site is correlated with

590   vehicle emissions, in fact the signature elements were Pb, Mn, Cu and EC.

591

4. Conclusions

The concentration and the chemical composition of PM_{10} in five cities within NW Europe showed significant spatial and seasonal variations. PM_{10} mass concentrations were higher at AP and the industrial sites than at the other urban sites. The concentration of SO_4^{2-}, NO_3^- and NH_4^+ was 68-81% of total WSIs, and around 32-37% of total PM_{10} concentration, indicating predominantly secondary sources of pollution. In addition, SO_4^{2-} was highest in summer suggesting photochemical formation. The seasonal variation of OC and EC in PM_{10} was similar in the five cities. The highest annual ratio of OC/EC was observed in AD (5.15), while the lowest value was found in AP (2.81). Crustal elements (Al, Ba, Ca, Fe, Mn, and Ti) dominated the identified elements of PM_{10}. EF values for Fe, Mn, Ti, Ba, and Ca are all less than 10 at the sampling sites (except WZ), suggesting that these elements are commonly derived from the crustal sources in this study. PM_{10} was highly enriched (EF>100) in As, Cd, Cu, Mo, Ni, Pb, Sn, and Zn at all sampling sites, indicating that these elements are associated with human activities (anthropogenic sources). The clear seasonal variations of MAs can be linked to the impact of biomass burning within residential heating (increased in winter), and also might be associated to different meteorological conditions. Mass closure allows for source understanding, quality assurance, health and environment effects. A large part of PM_{10} (31-36%) was attributed to secondary inorganic aerosol, and in particular to the nitrate-rich aerosol source profile, followed by OM and MD at four urban sites, and the major components of PM_{10} were SIA, followed by MD and SS at WZ site. UNK is generally attributed to the water content of PM which is associated with the estimation of the composition of crustal minerals and organic matter. PCA suggested the following sources: SIA, traffic emissions, marine aerosol, biomass burning, and industrial sources. The total sources explained 67.4, 80.3, 76.4, 73. 7, and 71.3% of the variance of the data at AD, AP, LL, WZ and LE sites, respectively. It can be concluded that the results in this study increase our understanding of the composition and sources of PM across NW Europe, which can enable the development of health-related air quality policies.

References

625

626 Adamo, P., Giordano, S., Sforza, A., Bargagli, R., 2011. Implementation of airborne trace

627 element monitoring with devitalised transplants of Hypnum cupressiforme Hedw.:

628 assessment of temporal trends and element contribution by vehicular traffic in Naples city.

629 Environ Pollut 159, 1620-1628.

630 Alastuey, A., Querol, X., Aas, W., Lucarelli, F., Pérez, N., Moreno, T., Cavalli, F., Areskoug,

631 H., Balan, V., Catrambone, M., Ceburnis, D., Cerro, J.C., Conil, S., Gevorgyan, L., Hueglin,

632 C., Imre, K., Jaffrezo, J.-L., Leeson, S.R., Mihalopoulos, N., Mitosinkova, M., apos, Dowd,

633 C.D., Pey, J., Putaud, J.-P., Riffault, V., Ripoll, A., Sciare, J., Sellegri, K., Spindler, G., Yttri,

634 K.E., 2016. Geochemistry of PM$_{10}$ over Europe during the EMEP intensive

635 measurement periods in summer 2012 and winter 2013. Atmospheric Chemistry and Physics

636 16, 6107-6129.

637 Almeida, T.S., Sant Ana, M.O., Cruz, J.M., Tormen, L., Frescura Bascunan, V.L.A.,

638 Azevedo, P.A., Garcia, C.A.B., Alves, J., Araujo, R.G.O., 2017. Characterisation and source

639 identification of the total airborne particulate matter collected in an urban area of Aracaju,

640 Northeast, Brazil. Environ Pollut 226, 444-451.

641 Amato, F., Favez, O., Pandolfi, M., Alastuey, A., Querol, X., Moukhtar, S., Bruge, B.,

642 Verlhac, S., Orza, J.A.G., Bonnaire, N., Le Priol, T., Petit, J.F., Sciare, J., 2016. Traffic

643 induced particle resuspension in Paris: Emission factors and source contributions.

644 Atmospheric Environment 129, 114-124.

645 Amato, F., Pandolfi, M., Escrig, A., Querol, X., Alastuey, A., Pey, J., Perez, N., Hopke, P.K.,

646 2009. Quantifying road dust resuspension in urban environment by Multilinear Engine: A

647 comparison with PMF2. Atmospheric Environment 43, 2770-2780.

648 AQEG, 2012. Fine Particulate Matter (PM2.5) in the United Kingdom, .

649 Bernardoni, V., Vecchi, R., Valli, G., Piazzalunga, A., Fermo, P., 2011. PM10 source

650 apportionment in Milan (Italy) using time-resolved data. Sci Total Environ 409, 4788-4795.

651 Bongiovanni, S.F., Prati , P., Zucchiatti, A., Lucarelli, F., Mando, P.A., Ariola, V., Bertone,

652 C., 2000. Study of the aerosol composition in the town of La Spezia with continuous

653 sampling and PIXE analysis. Nuclear Instruments and Methods in Physics Research B **161-

654 163**, 786-791.

655 Cao, J., Shen, Z., Chow, J.C., Qi, G., Watson, J.G., 2009. Seasonal variations and sources of

656 mass and chemical composition for PM10 aerosol in Hangzhou, China. Particuology 7, 161-

657 168.

658   Cesari, D., De Benedetto, G.E., Bonasoni, P., Busetto, M., Dinoi, A., Merico, E., Chirizzi, D.,

659   Cristofanelli, P., Donateo, A., Grasso, F.M., Marinoni, A., Pennetta, A., Contini, D., 2018.

660   Seasonal variability of PM2.5 and PM10 composition and sources in an urban background

661   site in Southern Italy. Sci Total Environ 612, 202-213.

662   Cesari, D., Donateo, A., Conte, M., Merico, E., Giangreco, A., Giangreco, F., Contini, D.,

663   2016a. An inter-comparison of PM2.5 at urban and urban background sites: Chemical

664   characterization and source apportionment. Atmospheric Research 174-175, 106-119.

665   Cesari, D., Genga, A., Ielpo, P., Siciliano, M., Mascolo, G., Grasso, F.M., Contini, D., 2014.

666   Source apportionment of PM(2.5) in the harbour-industrial area of Brindisi (Italy):

667   identification and estimation of the contribution of in-port ship emissions. Sci Total Environ

668   497-498, 392-400.

669   Chen, Y., Schleicher, N., Fricker, M., Cen, K., Liu, X.L., Kaminski, U., Yu, Y., Wu, X.F.,

670   Norra, S., 2016. Long-term variation of black carbon and PM2.5 in Beijing, China with

671   respect to meteorological conditions and governmental measures. Environ Pollut 212, 269-

672   278.

673   Ciaparra, D., Aries, E., Booth, M.-J., Anderson, D.R., Almeida, S.M., Harrad, S., 2009.

674   Characterisation of volatile organic compounds and polycyclic aromatic hydrocarbons in the

675   ambient air of steelworks. Atmospheric Environment 43, 2070-2079.

676   Contini, D., Donateo, A., Elefante, C., Grasso, F.M., 2012a. Analysis of particles and carbon

677   dioxide concentrations and fluxes in an urban area: Correlation with traffic rate and local

678   micrometeorology. Atmospheric Environment 46, 25-35.

679   Contini, D., Genga, A., Cesari, D., Siciliano, M., Donateo, A., Bove, M.C., Guascito, M.R.,

680   2010. Characterisation and source apportionment of PM10 in an urban background site in

681   Lecce. Atmospheric Research 95, 40-54.

682   Cordell, R.L., Mazet, M., Dechoux, C., Hama, S.M.L., Staelens, J., Hofman, J., Stroobants,

683   C., Roekens, E., Kos, G.P.A., Weijers, E.P., Frumau, K.F.A., Panteliadis, P., Delaunay, T.,

684   Wyche, K.P., Monks, P.S., 2016. Evaluation of biomass burning across North West Europe

685   and its impact on air quality. Atmos Environ 141, 276-286.

686   Cordell, R.L., White, I.R., Monks, P.S., 2014. Validation of an assay for the determination of

687   levoglucosan and associated monosaccharide anhydrides for the quantification of wood

688   smoke in atmospheric aerosol. Anal Bioanal Chem 406, 5283-5292.

689   Crilley, L.R., Lucarelli, F., Bloss, W.J., Harrison, R.M., Beddows, D.C., Calzolai, G., Nava,

690   S., Valli, G., Bernardoni, V., Vecchi, R., 2017. Source apportionment of fine and coarse

particles at a roadside and urban background site in London during the 2012 summer ClearfLo campaign. Environ Pollut 220, 766-778.

Cusack, M., Pérez, N., Pey, J., Alastuey, A., Querol, X., 2013. Source apportionment of fine PM and sub-micron particle number concentrations at a regional background site in the western Mediterranean: a 2.5 year study. Atmospheric Chemistry and Physics 13, 5173-5187.

de Kok, T.M., Driece, H.A., Hogervorst, J.G., Briede, J.J., 2006. Toxicological assessment of ambient and traffic-related particulate matter: a review of recent studies. Mutat Res 613, 103-122.

de Winter, J.C., Dodou, D., Wieringa, P.A., 2009. Exploratory Factor Analysis With Small Sample Sizes. Multivariate Behav Res 44, 147-181.

Dockery, D.W.a., Stone, P.H., 2007. Cardiovascular Risks from Fine Particulate Air Pollution. The New England Journal of Medicine 356(5), 511-513.

EC, 2004. Council Directive 2004/107/EC relating to arsenic, cadmium, mercury, nickel and polycyclic aromatic hydrocarbons in ambient air., pp. 3-16.

EEA, 2014. Air quality in Europe European Environment Agency, Luxemburg.

EEA, 2016. Air quality in Europe, European Environment Agency, Luxemburg.

Fuller, G.W., Tremper, A.H., Baker, T.D., Yttri, K.E., Butterfield, D., 2014. Contribution of wood burning to PM10 in London. Atmospheric Environment 87, 87-94.

Furuta, N., Iijima, A., Kambe, A., Sakai, K., Sato, K., 2005. Concentrations, enrichment and predominant sources of Sb and other trace elements in size classified airborne particulate matter collected in Tokyo from 1995 to 2004. J Environ Monit 7, 1155-1161.

Gray, H.A.a., Cass, G.R., 1986. Characteristics of Atmospheric Organic and Elemental Carbon Particle Concentrations in Los Angeles. Environ. Sci. Technol. 20, 580-589.

Gustafsson, M., Blomqvist, G., Gudmundsson, A., Dahl, A., Swietlicki, E., Bohgard, M., Lindbom, J., Ljungman, A., 2008. Properties and toxicological effects of particles from the interaction between tyres, road pavement and winter traction material. Sci Total Environ 393, 226-240.

Hama, S.M.L., Cordell, R.L., Kos, G.P.A., Weijers, E.P., Monks, P.S., 2017b. Sub-micron particle number size distribution characteristics at two urban locations in Leicester. Atmospheric Research 194, 1-16.

Hama, S.M.L., Cordell, R.L., Monks, P.S., 2017. Quantifying primary and secondary source contributions to ultrafine particles in the UK urban background. Atmos Environ 166, 62-78.

723   Hama, S.M.L., Ma, N., Cordell, R.L., Kos, G.P.A., Wiedensohler, A., Monks, P.S., 2017a.

724   Lung deposited surface area in Leicester urban background site/UK: Sources and contribution

725   of new particle formation. Atmospheric Environment 151, 94-107.

726   Harrison, R.M., Jones, A.M., Lawrence, R.G., 2003. A pragmatic mass closure model for

727   airborne particulate matter at urban background and roadside sites. Atmospheric Environment

728   37, 4927-4933.

729   Harrison, R.M., Yin, J., 2000. Particulate matter in the atmosphere: which particle properties

730   are important for its effects on health? The Science of the Total Environment 249, 85-101.

731   Heal, M.R., Kumar, P., Harrison, R.M., 2012. Particles, air quality, policy and health. Chem

732   Soc Rev 41, 6606-6630.

733   Ho, K.F., Lee, S.C., Yu, J.C., Zou, S.C., Fung, K., 2002. Carbonaceous characteristics of

734   atmospheric particulate matter in Hong Kong. The Science of the Total Environment 300, 59-

735   67.

736   Hoffman, D., Tilgner, A., Iinuma, Y., Herrmann, H., 2010. Atmospheric stability of

737   levoglucosan: a detailed laboratory and modeling study. Environ. Sci. Technol. 44, 694-699.

738   Hofman, J., Staelens, J., Cordell, R., Stroobants, C., Zikova, N., Hama, S.M.L., Wyche, K.P.,

739   Kos, G.P.A., Van Der Zee, S., Smallbone, K.L., Weijers, E.P., Monks, P.S., Roekens, E.,

740   2016. Ultrafine particles in four European urban environments: Results from a new

741   continuous long-term monitoring network. Atmos Environ 136, 68-81.

742   Hopke, P.K., 2000. A guide to positive matrix factorization, U.S. Environmental Protection

743   Agency, Research Triangle Park, NC 27711, USA.

744   IPCC, 2008. Climate Change 2007 Synthesis Report.

745   Isaksen, I.S.A., Granier, C., Myhre, G., Berntsen, T.K., Dalsoren, S.B., Gauss, M., Klimont,

746   Z., Benestad, R., Bousquet, P., Collins, W., Cox, T., Eyring, V., Fowler, D., Fuzzi, S., Jockel,

747   P., Laj, P., Lohmann, U., Maione, M., Monks, P., Prevot, A.S.H., Raes, F., Richter, A.,

748   Rognerud, B., Schulz, M., Shindell, D., Stevenson, D.S., Storelvmo, T., Wang, W.C., van

749   Weele, M., Wild, M., Wuebbles, D., 2009. Atmospheric composition change: Climate-

750   Chemistry interactions. Atmos Environ 43, 5138-5192.

751   Jeong, C.H., Evans, G.J., McGuire, M.L., Chang, R.Y.W., Abbatt, J.P.D., Zeromskiene, K.,

752   Mozurkewich, M., Li, S.M., Leaitch, W.R., 2010. Particle formation and growth at five rural

753   and urban sites. Atmospheric Chemistry and Physics 10, 7979-7995.

754   Joaquin, 2015. Composition and source apportionment of PM10. Joint Air Quality Initiative,

755   Work Package 1 Action 2 and 3, Flanders Environment Agency, Aalst. Available at

756   http://joaquin.eu.

757   Kelly, F.J., Fussell, J.C., 2012. Size, source and chemical composition as determinants of

758   toxicity attributable to ambient particulate matter. Atmospheric Environment 60, 504-526.

759   Kim, K.-H., Lee, J.-H., Jang, M.-S., 2002. Metals in airborne particulate matter from the first

760   and second industrial complex area of Taejon city, Korea. Environ Pollut 118, 41-51.

761   Krudysz, M., Moore, K., Geller, M., Sioutas, C., Froines, J., 2009. Intra-community spatial

762   variability of particulate matter size distributions in Southern California/Los Angeles. Atmos.

763   Chem. Phys. 9, 1061-1075.

764   Lawrence, S., Sokhi, R., Ravindra, K., Mao, H., Prain, H.D., Bull, I.D., 2013. Source

765   apportionment of traffic emissions of particulate matter using tunnel measurements.

766   Atmospheric Environment 77, 548-557.

767   Lin, Y.C., Tsai, C.J., Wu, Y.C., Zhang, R., Chi, K.H., Huang, Y.T., Lin, S.H., Hsu, S.C.,

768   2015. Characteristics of trace metals in traffic-derived particles in Hsuehshan Tunnel,

769   Taiwan: size distribution, potential source, and fingerprinting metal ratio. Atmospheric

770   Chemistry and Physics 15, 4117-4130.

771   Liu, B., Wu, J., Zhang, J., Wang, L., Yang, J., Liang, D., Dai, Q., Bi, X., Feng, Y., Zhang, Y.,

772   Zhang, Q., 2017. Characterization and source apportionment of PM2.5 based on error

773   estimation from EPA PMF 5.0 model at a medium city in China. Environ Pollut 222, 10-22.

774   Maenhaut, W., Vermeylen, R., Claeys, M., Vercauteren, J., Roekens, E., 2016. Sources of the

775   PM10 aerosol in Flanders, Belgium, and re-assessment of the contribution from wood

776   burning. Sci Total Environ 562, 550-560.

777   Mari, M., Harrison, R.M., Schuhmacher, M., Domingo, J.L., Pongpiachan, S., 2010.

778   Inferences over the sources and processes affecting polycyclic aromatic hydrocarbons in the

779   atmosphere derived from measured data. Sci Total Environ 408, 2387-2393.

780   McNeilly, J.D., Heal, M.R., Beverland, I.J., Howe, A., Gibson, M.D., Hibbs, L.R., MacNee,

781   W., Donaldson, K., 2004. Soluble transition metals cause the pro-inflammatory effects of

782   welding fumes in vitro. Toxicol Appl Pharmacol 196, 95-107.

783   Meister, K., Johansson, C., Forsberg, B., 2012. Estimated short-term effects of coarse

784   particles on daily mortality in Stockholm, Sweden. Environ Health Perspect 120, 431-436.

785   Mooibroek, D., Schaap, M., Weijers, E.P., Hoogerbrugge, R., 2011. Source apportionment

786   and spatial variability of PM2.5 using measurements at five sites in the Netherlands.

787   Atmospheric Environment 45, 4180-4191.

788   Moreno, T., Merolla, L., Gibbons, W., Greenwell, L., Jones, T., Richards, R., 2004.

789   Variations in the source, metal content and bioreactivity of technogenic aerosols: a case study

790   from Port Talbot, Wales, UK. Sci Total Environ 333, 59-73.

791   Muránszky, G., Óvári, M., Virág, I., Csiba, P., Dobai, R., Záray, G., 2011. Chemical

792   characterization of PM10 fractions of urban aerosol. Microchemical Journal 98, 1-10.

793   Nava, S., Becagli, S., Calzolai, G., Chiari, M., Lucarelli, F., Prati, P., Traversi, R., Udisti, R.,

794   Valli, G., Vecchi, R., 2012. Saharan dust impact in central Italy: An overview on three years

795   elemental data records. Atmospheric Environment 60, 444-452.

796   Pinto, J.P., Lefohn, A.S., Shadwick, D.S., 2004. Spatial Variability of PM2.5in Urban Areas

797   in the United States. Journal of the Air & Waste Management Association 54, 440-449.

798   Pope, C.A., and, Dockery, D.W., 2006. Health Effects of Fine Particulate Air Pollution: Lines

799   that Connect. Air & Waste Manage. Assoc. 56, 709-742.

800   Putaud, J.-P., Raes, F., Van Dingenen, R., Brüggemann, E., Facchini, M.C., Decesari, S.,

801   Fuzzi, S., Gehrig, R., Hüglin, C., Laj, P., Lorbeer, G., Maenhaut, W., Mihalopoulos, N.,

802   Müller, K., Querol, X., Rodriguez, S., Schneider, J., Spindler, G., Brink, H.t., Tørseth, K.,

803   Wiedensohler, A., 2004. A European aerosol phenomenology—2: chemical characteristics of

804   particulate matter at kerbside, urban, rural and background sites in Europe. Atmospheric

805   Environment 38, 2579-2595.

806   Querol, X., Alastuey, A., Moreno, T., Viana, M.M., Castillo, S., Pey, J., Rodríguez, S.,

807   Artiñano, B., Salvador, P., Sánchez, M., Garcia Dos Santos, S., Herce Garraleta, M.D.,

808   Fernandez-Patier, R., Moreno-Grau, S., Negral, L., Minguillón, M.C., Monfort, E., Sanz,

809   M.J., Palomo-Marín, R., Pinilla-Gil, E., Cuevas, E., de la Rosa, J., Sánchez de la Campa, A.,

810   2008. Spatial and temporal variations in airborne particulate matter (PM10 and PM2.5) across

811   Spain 1999–2005. Atmospheric Environment 42, 3964-3979.

812   Querol, X., Minguillón, M.C., Alastuey, A., Monfort, E., Mantilla, E., Sanz, M.J., Sanz, F.,

813   Roig, A., Renau, A., Felis, C., Miró, J.V., Artíñano, B., 2007. Impact of the implementation

814   of PM abatement technology on the ambient air levels of metals in a highly industrialised

815   area. Atmospheric Environment 41, 1026-1040.

816   Rees, S.L., Robinson, A.L., Khlystov, A., Stanier, C.O., Pandis, S.N., 2004. Mass balance

817   closure and the Federal Reference Method for PM2.5 in Pittsburgh, Pennsylvania.

818   Atmospheric Environment 38, 3305-3318.

819   Rodriguez, S., Querol, X., Alastuey, A., Viana, M., Alarcon, M., Mantilla, E., Ruiz, C., 2004.

820   Comparative PM10–PM2.5 source contribution study at rural, urban and industrial sites

821   during PM episodes in Eastern Spain. Science of The Total Environment 328, 95-113.

822   Röösli , M., Theis, G., Künzli, N., Staehelin, J., Mathys, P., Oglesby, L., Camenzind, M.,

823   Braun-Fahrländer, C., 2001. Temporal and spatial variation of the chemical composition of

824   PM10 at urban and rural sites in the Basel area, Switzerland. Atmospheric Environment 35,

825   3701-3713.

826   Safai, P.D., Raju, M.P., Rao, P.S.P., Pandithurai, G., 2014. Characterization of carbonaceous

827   aerosols over the urban tropical location and a new approach to evaluate their climatic

828   importance. Atmospheric Environment 92, 493-500.

829   Saffari, A., Daher, N., Shafer, M.M., Schauer, J.J., Sioutas, C., 2013. Seasonal and spatial

830   variation of trace elements and metals in quasi-ultrafine (PM(0).(2)(5)) particles in the Los

831   Angeles metropolitan area and characterization of their sources. Environ Pollut 181, 14-23.

832   Samiksha, S., Sunder Raman, R., Nirmalkar, J., Kumar, S., Sirvaiya, R., 2017. PM10 and

833   PM2.5 chemical source profiles with optical attenuation and health risk indicators of paved

834   and unpaved road dust in Bhopal, India. Environ Pollut 222, 477-485.

835   Schauer, J.J., Kleeman, M.J., Cass, G.R., Simoneit, B.R., 2002. Measurement of Emissions

836   from Air Pollution Sources. 5. C1-C32 Organic Compounds from Gasoline-Powered Motor

837   Vehicles. Environ. Sci. Technol. 36, 1169-1180.

838   Seinfeld, J.H., and, Pandis, S.N., 2006. Atmospheric Chemistry and Physics: From Air

839   Pollution to Climate Change, Second ed, John Wiley and Sons. Inc., New York.

840   Shi, G.-L., Zeng, F., Li, X., Feng, Y.-C., Wang, Y.-Q., Liu, G.-X., Zhu, T., 2011. Estimated

841   contributions and uncertainties of PCA/MLR–CMB results: Source apportionment for

842   synthetic and ambient datasets. Atmospheric Environment 45, 2811-2819.

843   Simoneit, B.R.T., Schauer, J.J., Nolte, C.G., Oros, D.R., Elias, V.O., Fraser, M.P., Rogge,

844   W.F., Cass, G.R., 1999. Levoglucosan, a tracer for cellulose in biomass burning and

845   atmospheric particles. Atmospheric Environment 33, 173-182.

846   Taiwo, A.M., Beddows, D.C., Calzolai, G., Harrison, R.M., Lucarelli, F., Nava, S., Shi, Z.,

847   Valli, G., Vecchi, R., 2014a. Receptor modelling of airborne particulate matter in the vicinity

848   of a major steelworks site. Sci Total Environ 490, 488-500.

849   Taiwo, A.M., Beddows, D.C., Shi, Z., Harrison, R.M., 2014b. Mass and number size

850   distributions of particulate matter components: comparison of an industrial site and an urban

851   background site. Sci Total Environ 475, 29-38.

852   Taiwo, A.M., Harrison, R.M., Beddows, D.C.S., Shi, Z., 2014c. Source apportionment of

853   single particles sampled at the industrially polluted town of Port Talbot, United Kingdom by

854   ATOFMS. Atmospheric Environment 97, 155-165.

855   Takahashi, K., Minoura, H., Sakamoto, K., 2008. Chemical composition of atmospheric

856   aerosols in the general environment and around a trunk road in the Tokyo metropolitan area.

857   Atmospheric Environment 42, 113-125.

858   Terzi, E., Argyropoulos, G., Bougatioti, A., Mihalopoulos, N., Nikolaou, K., Samara, C.,

859   2010. Chemical composition and mass closure of ambient PM10 at urban sites. Atmospheric

860   Environment 44, 2231-2239.

861   Thorpe, A., Harrison, R.M., 2008. Sources and properties of non-exhaust particulate matter

862   from road traffic: a review. Sci Total Environ 400, 270-282.

863   Tsyro, S.G., 2005. To what extent can aerosol water explain the discrepancy between model

864   calculated and gravimetric PM10 and PM2.5? Atmos. Chem. Phys. 5, 515-532.

865   Turner, J.R., and, Allen, D.T., 2008. Transport of Atmospheric Fine Particulate Matter: Part

866   2—Findings from Recent Field Programs on the Intraurban Variability in Fine Particulate

867   Matter. Journal of the Air & Waste Management Association 58, 196-215.

868   Turpin, B.J., and, Lim, H.-J., 2001. Species Contributions to PM2.5 Mass Concentrations:

869   Revisiting Common Assumptions for Estimating Organic Mass. Aerosol Science and

870   Technology 35, 602-610.

871   Vecchi, R., Chiari, M., D'Alessandro, A., Fermo, P., Lucarelli, F., Mazzei, F., Nava, S.,

872   Piazzalunga, A., Prati, P., Silvani, F., Valli, G., 2008. A mass closure and PMF source

873   apportionment study on the sub-micron sized aerosol fraction at urban sites in Italy.

874   Atmospheric Environment 42, 2240-2253.

875   Vercauteren, J., Matheeussen, C., Wauters, E., Roekens, E., van Grieken, R., Krata, A.,

876   Makarovska, Y., Maenhaut, W., Chi, X., Geypens, B., 2011. Chemkar PM10: An extensive

877   look at the local differences in chemical composition of PM10 in Flanders, Belgium.

878   Atmospheric Environment 45, 108-116.

879   Viana, M., Maenhaut, W., Chi, X., Querol, X., Alastuey, A., 2007. Comparative chemical

880   mass closure of fine and coarse aerosols at two sites in south and west Europe: Implications

881   for EU air pollution policies. Atmospheric Environment 41, 315-326.

882   Waked, A., Favez, O., Alleman, L.Y., Piot, C., Petit, J.E., Delaunay, T., Verlinden, E., Golly,

883   B., Besombes, J.L., Jaffrezo, J.L., Leoz-Garziandia, E., 2014. Source apportionment of

884   PM_{10} in a north-western Europe regional urban background site (Lens, France)

885   using positive matrix factorization and including primary biogenic emissions. Atmospheric

886   Chemistry and Physics 14, 3325-3346.

887   Wang, H., Kawamura, K., Shooter, D., 2005. Carbonaceous and ionic components in

888   wintertime atmospheric aerosols from two New Zealand cities: Implications for solid fuel

889   combustion. Atmospheric Environment 39, 5865-5875.

890   Wedepohl, K.H., 1995. The composition of the continental crust. Geochimica et

891   Cosmochimica Acta 59, 1217-1232.

892 Weijers, E.P., Schaap, M., Nguyen, L., Matthijsen, J., Denier van der Gon, H.A.C., ten Brink,
893 H.M., Hoogerbrugge, R., 2011. Anthropogenic and natural constituents in particulate matter
894 in the Netherlands. Atmospheric Chemistry and Physics 11, 2281-2294.
895 WHO, 2005. Air quality guidelines. Global update 2005. Particulate matter, ozone, nitrogen
896 dioxide and sulfur dioxide., Regional Office for Europe, Copenhagen.
897 Wilson, J.G., Kingham, S., Pearce, J., Sturman, A.P., 2005. A review of intraurban variations
898 in particulate air pollution: Implications for epidemiological research. Atmospheric
899 Environment 39, 6444-6462.
900 Wongphatarakul, V., Friedlander, S.K., Pinto, J.P., 1998. A Comparative Study of PM2.5
901 Ambient Aerosol Chemical Databases. Environ. Sci. Technol. 32, 3926-3934.
902
903
904
905
906
907
908
909
910
911
912
913
914
915
916

917   Table 1: Location and characteristics of the five PM$_{10}$ sampling sites.

918

City	Site name	Latitude	Longitude	Distance to main street (m)	Traffic Intensity (Vehicles/day)
Amsterdam (AD)	Vondelpark	52° 21′ 35″ N	4° 51′ 59″ E	64	17000
Antwerp (AP)	Borgerhout	51° 12′ 35″ N	4° 25′ 55″ E	30	29500
Leicester (LE)	University of Leicester	52° 37′ 12″ N	1° 07′ 38″ W	140	22500
Lille (LL)	Lille Fives	50° 37′ 41″ N	3° 05′ 25″ E	35	NA
Wijk aan Zee (WZ)	Wijk aan Zee	52° 49′ 40″ N	4° 60′ 23″ E	70	NA

919

920

921

922

923

924

925

926

927

928

929

930

931

932

933

934

935

936

937

938

939

940

941 Table 2: PM$_{10}$ mass concentration (μg m^{-3}) at the five sites, (n= number of samples).

942

	AD			AP			LE		
	Annual	Cold Period	Warm Period	Annual	Cold Period	Warm Period	Annual	Cold Period	Warm Period
Average	20.71	24.24	17.65	24.92	28.11	22.1	16.16	18.33	14.45
Max	84.9	84.9	54.62	100.06	100.06	62.43	76.61	76.61	44.96
Median	18.2	20.81	16.23	21.25	24.32	19.92	13.47	14.96	13
Min	6.28	6.28	7.72	7.16	7.16	9.65	2.27	4.42	5.15
St. dev.	10.61	12.81	6.51	12.13	14.59	8.45	9.6	12.09	6.51
n	354	204	180	353	200	184	327	172	184
	LL			WZ					
Average	22.4	23.23	21.66	25.6	31.2	20.52			
Max	98	98	63.49	81.4	89.22	52.19			
Median	18.39	18.47	18.47	23.77	28.88	18.27			
Min	4.14	6.25	4.14	4.34	4.34	6.05			
St. dev.	13.32	15.3	10.7	12.68	14.35	8.85			
n	327	173	126	340	195	174			

943

944

945 Table 3: Coefficients of divergence (COD) of the daily PM$_{10}$ mass concentrations (μg m^{-3})
946 between the monitoring sites.

COD					
	AD	AP	LE	LL	WZ
AD	0	0.162	0.24	0.204	0.192
AP		0	0.294	0.155	0.231
LE			0	0.277	0.342
LL				0	0.301
WZ					0

947

948

949 Table 4: The ratios of NO_3^-/PM_{10}, SO_4^{2-}/PM_{10}, and SO_4^{2-}/NO_3^- in PM_{10} at five sampling sites

950 during different periods.

	AD			AP			LE		
	Annual	Cold Period	Warm Period	Annual	Cold Period	Warm Period	Annual	Cold Period	Warm Period
NO_3^-/PM_{10}	0.202	0.233	0.147	0.205	0.237	0.154	0.177	0.213	0.118
SO_4^{2-}/PM_{10}	0.0926	0.075	0.123	0.083	0.067	0.107	0.0955	0.078	0.1244
SO_4^{2-}/NO_3^-	0.457	0.324	0.835	0.403	0.285	0.694	0.538	0.366	1.055

	LL			WZ		
NO_3^-/PM_{10}	0.220	0.26	0.119	0.172	0.189	0.129
SO_4^{2-}/PM_{10}	0.081	0.0754	0.097	0.096	0.084	0.129
SO_4^{2-}/NO_3^-	0.367	0.290	0.813	0.560	0.443	0.994

951

952

953

954

955

956

957

958

959

960

961

962

963

964

Table 5: PM_{10} mass closure results ($\mu g\ m^{-3}$) at sampling sites.

| | AD | | | AP | | | LE | | |
	Annual	Cold Period	Warm Period	Annual	Cold Period	Warm Period	Annual	Cold Period	Warm Period
MD	2.26	2.19	2.21	3.79	4.77	3.09	2.05	2.20	1.88
OM	4.22	4.46	3.95	6.15	6.99	5.26	4.75	5.07	4.38
EC	0.58	0.65	0.51	1.56	1.81	1.29	0.95	1.16	0.72
TE	0.12	0.11	0.12	0.19	0.23	0.17	0.10	0.098	0.10
SS	2.80	3.18	2.37	2.51	3.09	1.9	2.93	3.84	1.89
SIA	8.52	11.1	5.61	10.52	13.6	7.28	6.23	8.01	4.23
MSS	0.066	0.11	0.021	0.13	0.20	0.06	0.074	0.11	0.032
UNK	5.13	6.85	3.08	5.58	5.8	5.02	2.23	2.26	2.2

	LL			WZ		
MD	3.38	4.2	2.57	5.58	6.7	3.94
OM	6.26	6.95	5.33	3.94	4.33	3.4
EC	1.19	1.31	1.02	0.81	1.02	0.53
TE	0.16	0.17	0.15	0.18	0.19	0.17
SS	2.3	2.6	1.76	4.57	5.33	3.52
SIA	10.85	13.44	6.07	9.16	11.84	5.5
MSS	0.2	0.34	0.04	0.064	0.097	0.019
UNK	5.43	3.66	7.39	4.73	6.56	2.36

Table 6: Factor loadings for PM$_{10}$ at AD, AP, LL, WZ and LE.

	AD					AP					LL					WZ					LE			
Variable	PC1	PC2	PC3	PC4	PC5	PC1	PC2	PC3	PC4	PC5	PC1	PC2	PC3	PC4	PC5	PC1	PC2	PC3	PC4	PC5	PC1	PC2	PC3	PC4
NO$_3^-$	0.031	**0.745**	0.032	0.035	0.003	0.038	**0.658**	0.023	0.077	0.04	0.028	**0.79**	0.031	0.068	0.028	0.01	**0.819**	0.018	0.022	0.001	0.00	**0.748**	0.014	0.116
Cl$^-$	0.006	0.005	**0.834**	0.002	0.027	0.017	0.005	**0.907**	0.004	0.00	0.048	0.002	**0.862**	0.001	0.048	0.016	0.051	**0.761**	0.00	0.061	0.015	0.012	**0.915**	0.006
SO$_4^{2-}$	0.04	**0.302**	0.098	0.185	0.014	0.068	**0.66**	0.023	0.004	0.03	0.097	**0.675**	0.053	0.000	0.097	0.053	**0.471**	0.034	0.129	0.039	0.056	**0.737**	0.004	0.002
Na$^+$	0.001	0.043	**0.852**	0.015	0.024	0.028	0.027	**0.913**	0.000	0.001	0.053	0.042	**0.857**	0.001	0.053	0.014	0.09	**0.743**	0.01	0.031	0.022	0.019	**0.934**	0.003
NH$_4^+$	0.007	**0.736**	0.066	0.07	0.006	0.017	**0.73**	0.035	0.07	0.025	0.018	**0.829**	0.036	0.045	0.018	0.001	**0.796**	0.042	0.068	0.002	0.000	**0.803**	0.024	0.086
K$^+$	0.006	0.007	0.057	**0.791**	0.000	0.005	0.005	**0.947**	0.006	0.005	0.004	0.02	**0.857**	0.007	0.004	0.000	0.06	**0.662**	0.035	0.116	0.005	0.007	**0.948**	0.002
Mg^{2+}	0.007	0.02	**0.751**	0.013	0.000	**0.817**	0.014	0.002	0.000	0.034	**0.567**	0.054	0.009	0.004	**0.567**	0.506	0.04	0.093	0.005	0.011	**0.577**	0.029	0.001	0.096
Al	**0.633**	0.196	0.032	0.000	0.196	0.003	0.112	0.011	0.073	**0.518**	0.098	**0.438**	0.029	0.14	0.098	0.001	0.092	0.07	0.259	0.123	0.015	0.056	0.001	**0.481**
As	0.000	0.184	0.012	**0.563**	0.059	0.057	0.018	0.000	0.055	**0.614**	**0.358**	0.048	0.013	0.164	**0.358**	0.294	0.032	0.000	0.007	0.004	0.168	0.015	0.000	**0.544**
Ba	**0.643**	0.055	0.025	0.014	0.003	**0.867**	0.043	0.001	0.002	0.01	**0.637**	0.144	0.041	0.001	**0.637**	**0.793**	0.000	0.000	0.001	0.003	**0.651**	0.021	0.000	0.001
Ca	**0.788**	0.000	0.016	0.003	0.001	0.001	0.054	0.016	0.111	0.241	0.008	0.003	0.002	0.001	0.008	0.036	0.006	0.005	0.02	**0.611**	0.072	0.046	0.01	0.232
Cd	0.001	0.133	0.000	**0.691**	0.003	0.163	0.029	0.002	0.033	**0.315**	**0.562**	0.000	0.01	0.023	**0.562**	0.002	0.003	0.001	0.059	0.194	0.228	0.061	0.008	0.039
Cr	0.121	0.007	0.169	0.001	0.065	0.042	0.009	0.008	0.052	**0.798**	**0.430**	0.000	0.005	0.255	**0.43**	0.018	0.058	0.205	0.000	0.065	0.182	0.06	0.008	**0.532**
Cu	0.000	0.026	0.009	0.01	**0.653**	0.115	0.029	0.001	0.075	**0.708**	**0.588**	0.057	0.005	0.102	**0.588**	0.022	0.003	0.000	0.087	**0.758**	0.205	0.000	0.027	**0.517**
Fe	0.003	**0.463**	0.001	0.033	0.172	0.100	0.122	0.001	0.217	0.234	**0.739**	0.229	0.106	0.183	0.239	0.045	0.001	0.041	0.253	**0.457**	0.147	0.048	0.093	0.29
Mn	0.001	0.011	0.000	0.003	0.05	0.176	0.084	0.001	0.023	**0.548**	**0.623**	0.021	0.014	0.000	0.223	0.031	0.001	0.005	0.003	**0.789**	0.093	0.018	0.000	0.136
Mo	0.013	0.165	0.019	0.011	0.227	0.03	0.09	0.001	0.04	**0.673**	0.239	0.215	0.000	0.086	0.239	0.116	0.227	0.049	0.003	**0.367**	0.236	0.001	0.015	**0.396**
Ni	0.002	0.000	0.01	0.001	**0.643**	0.045	0.263	0.001	0.092	0.238	0.264	0.136	0.004	0.000	0.264	0.039	0.004	0.037	0.135	0.043	0.091	0.000	0.000	0.018
Pb	0.000	0.026	0.019	0.165	0.002	0.000	0.164	0.007	0.087	**0.427**	0.121	**0.438**	0.038	0.134	0.121	0.008	0.005	0.002	0.022	**0.789**	0.001	0.043	0.006	0.266
Sb	0.002	0.01	0.008	0.004	0.043	0.003	0.194	0.000	0.028	**0.457**	0.023	0.001	0.004	0.044	0.023	0.001	0.02	0.231	0.164	0.037	0.014	0.012	0.009	**0.741**
Ti	**0.596**	0.061	0.046	0.000	0.283	**0.825**	0.021	0.006	0.000	0.048	**0.669**	0.094	0.039	0.02	**0.669**	**0.539**	0.022	0.038	0.021	0.15	**0.709**	0.076	0.033	0.002
V	0.009	**0.451**	0.004	0.003	**0.549**	0.09	**0.424**	0.001	0.04	0.086	0.18	**0.392**	0.003	0.000	0.180	0.100	0.221	0.007	0.094	0.214	0.142	**0.444**	0.002	0.013
Zn	**0.318**	0.000	0.108	0.001	0.151	**0.377**	0.1	0.048	0.046	0.003	**0.459**	0.08	0.101	0.000	**0.459**	**0.564**	0.013	0.003	0.001	0.144	**0.666**	0.061	0.028	0.000
Gal.	0.004	0.004	0.000	**0.910**	0.002	0.000	0.022	0.000	**0.704**	0.23	0.032	0.023	0.000	**0.842**	0.032	0.005	0.015	0.000	**0.695**	0.001	0.000	0.065	0.000	**0.785**
Man.	0.000	0.003	0.007	**0.922**	0.001	0.021	0.032	0.001	**0.743**	0.158	0.003	0.057	0.002	**0.816**	0.003	0.000	0.009	0.012	**0.855**	0.014	0.001	0.037	0.001	**0.811**
Lev	0.001	0.011	0.005	**0.857**	0.000	0.005	0.011	0.001	**0.721**	0.202	0.002	0.022	0.000	**0.887**	0.002	0.001	0.014	0.004	**0.863**	0.024	0.000	0.045	0.000	**0.809**
OC	0.014	0.123	0.103	**0.631**	0.058	0.068	0.164	0.094	0.181	**0.360**	0.179	0.255	0.076	**0.339**	0.179	0.012	0.171	0.156	**0.526**	0.03	0.092	0.137	0.031	**0.597**
EC	0.000	**0.316**	0.033	0.11	0.03	0.002	0.003	0.001	0.114	**0.746**	0.148	0.003	0.000	**0.576**	0.148	0.001	0.055	0.000	0.013	**0.655**	0.031	0.022	0.007	**0.779**

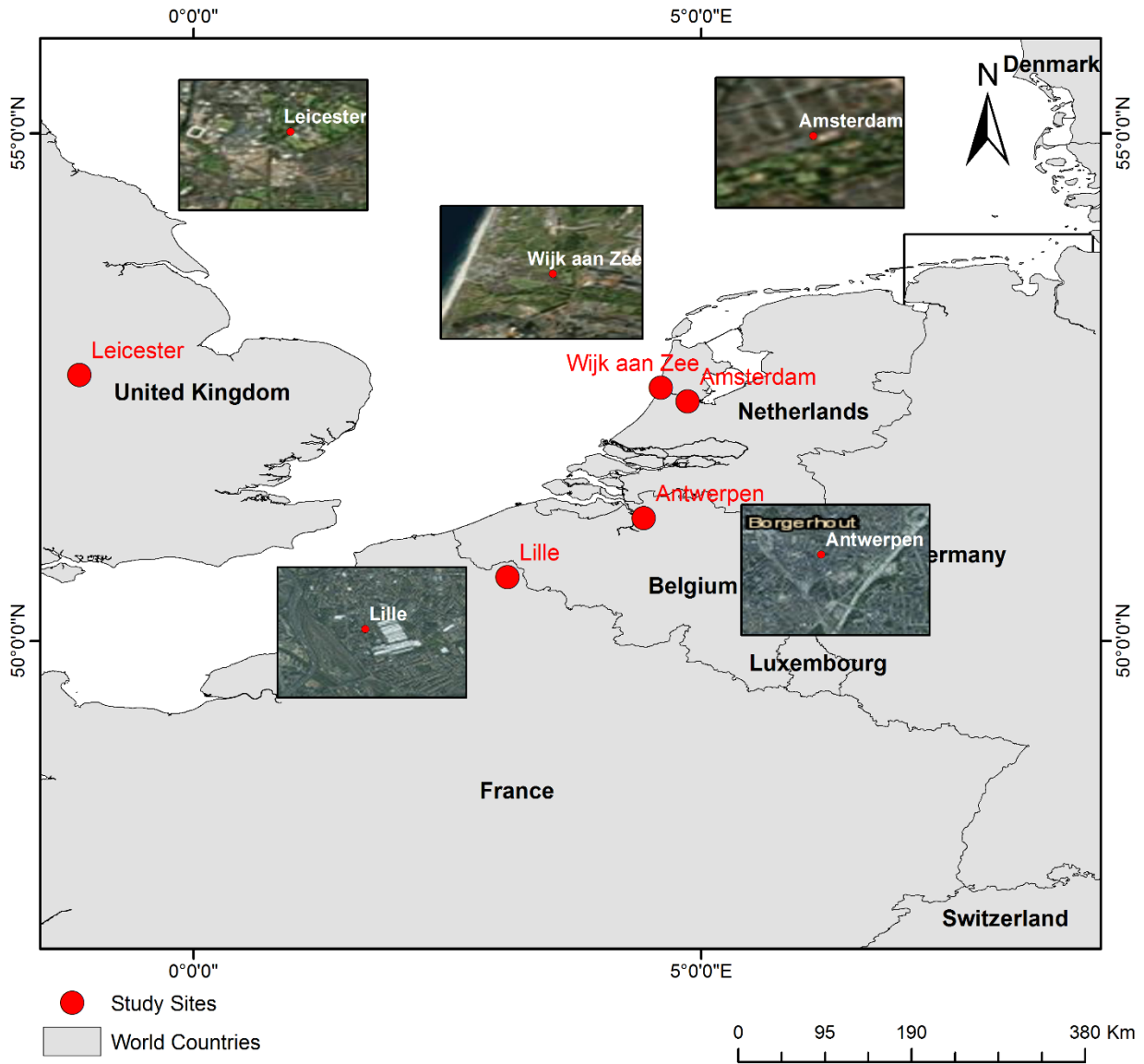Loads larger than 0.3 (in absolute values) are reported in bold
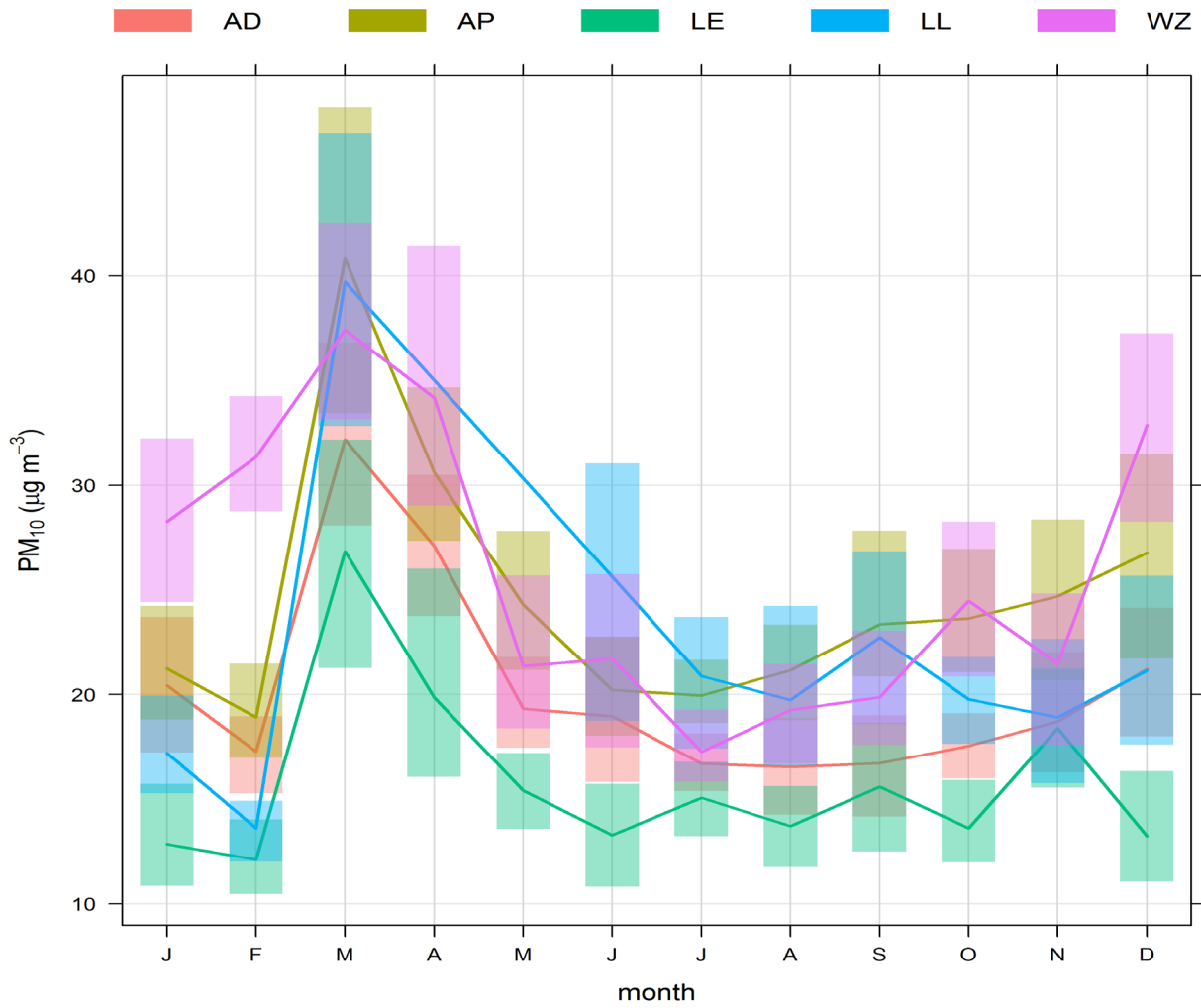
Figure 1: Map of the locations of all monitoring sites.

Figure 2: Monthly variations of PM$_{10}$ concentrations at the sampling sites. Different colours in the bars show PM$_{10}$ percentage for each site with monthly variations, and lines show monthly concertation of PM$_{10}$.
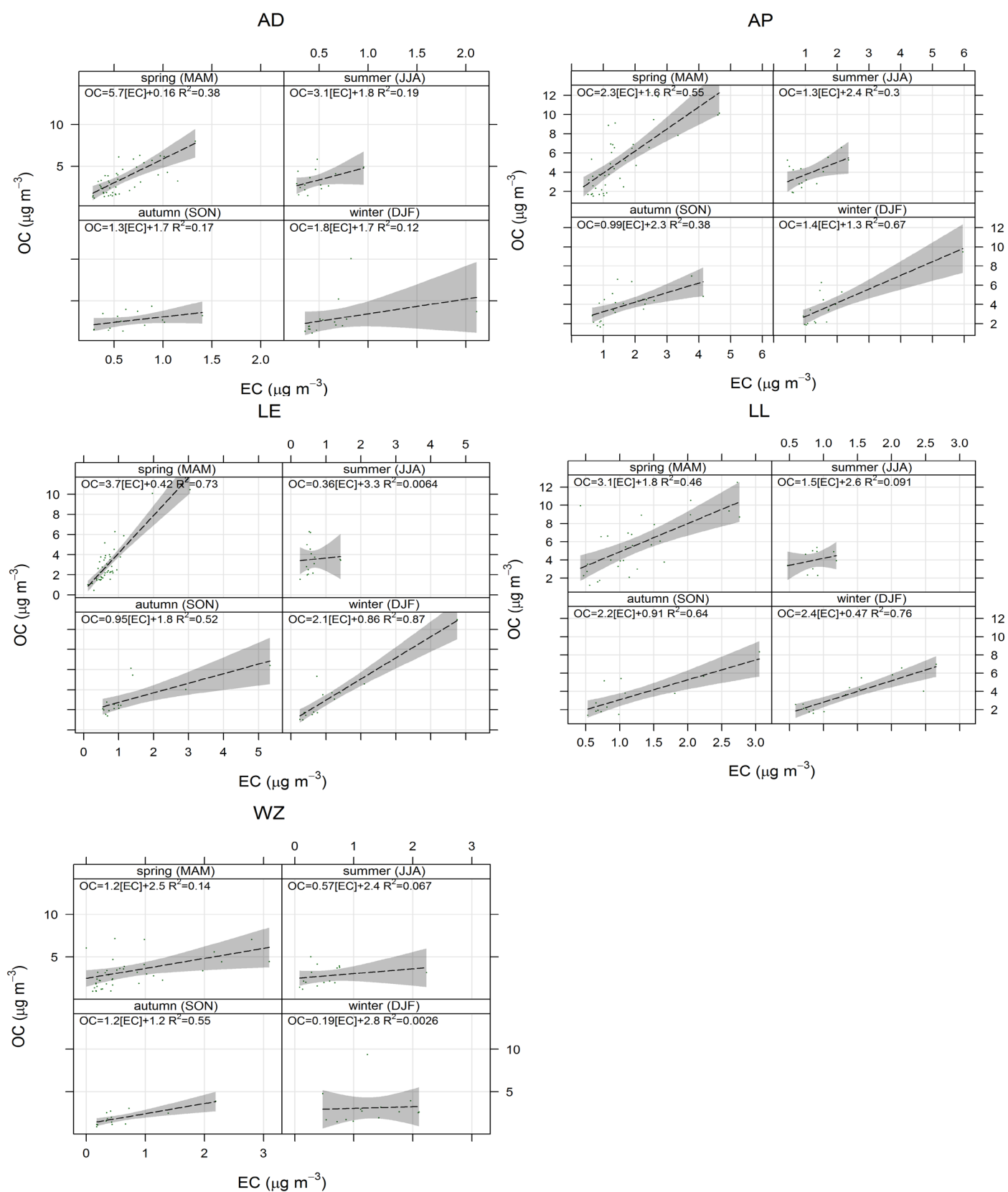
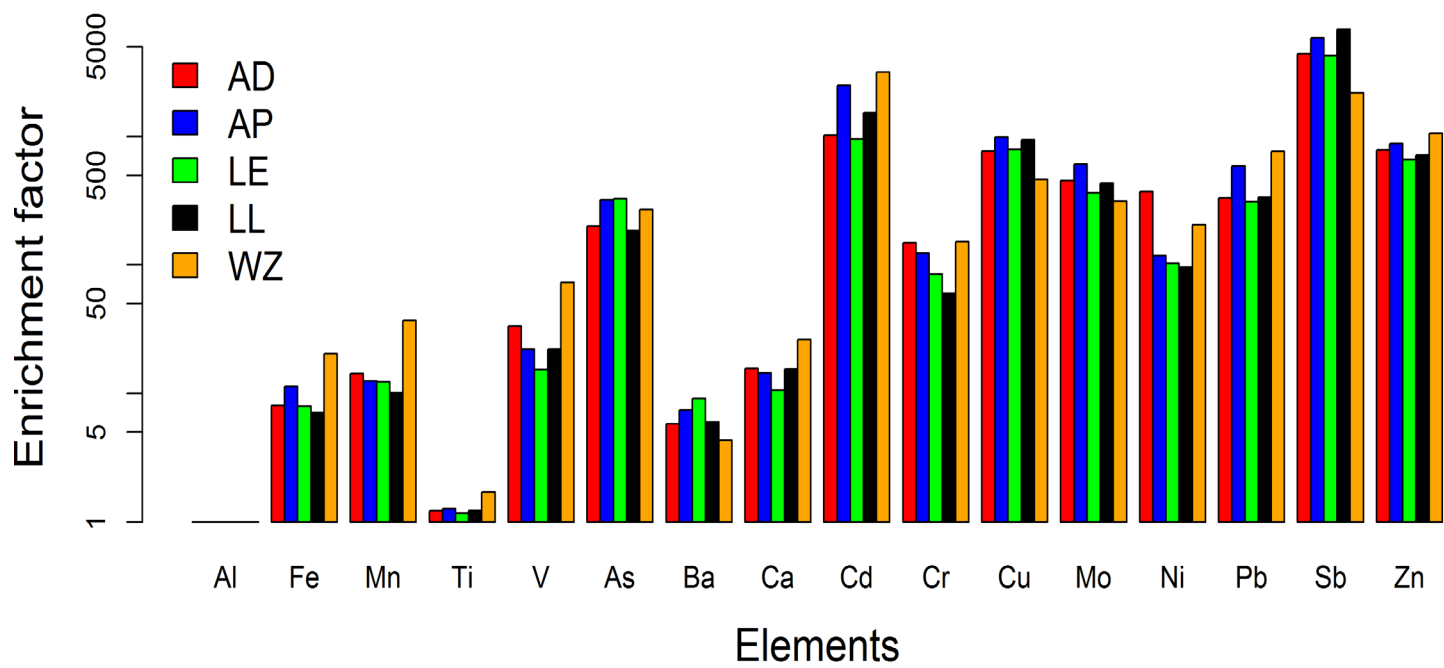Figure 3: Correlations between OC and EC during different seasons at all sampling sites.

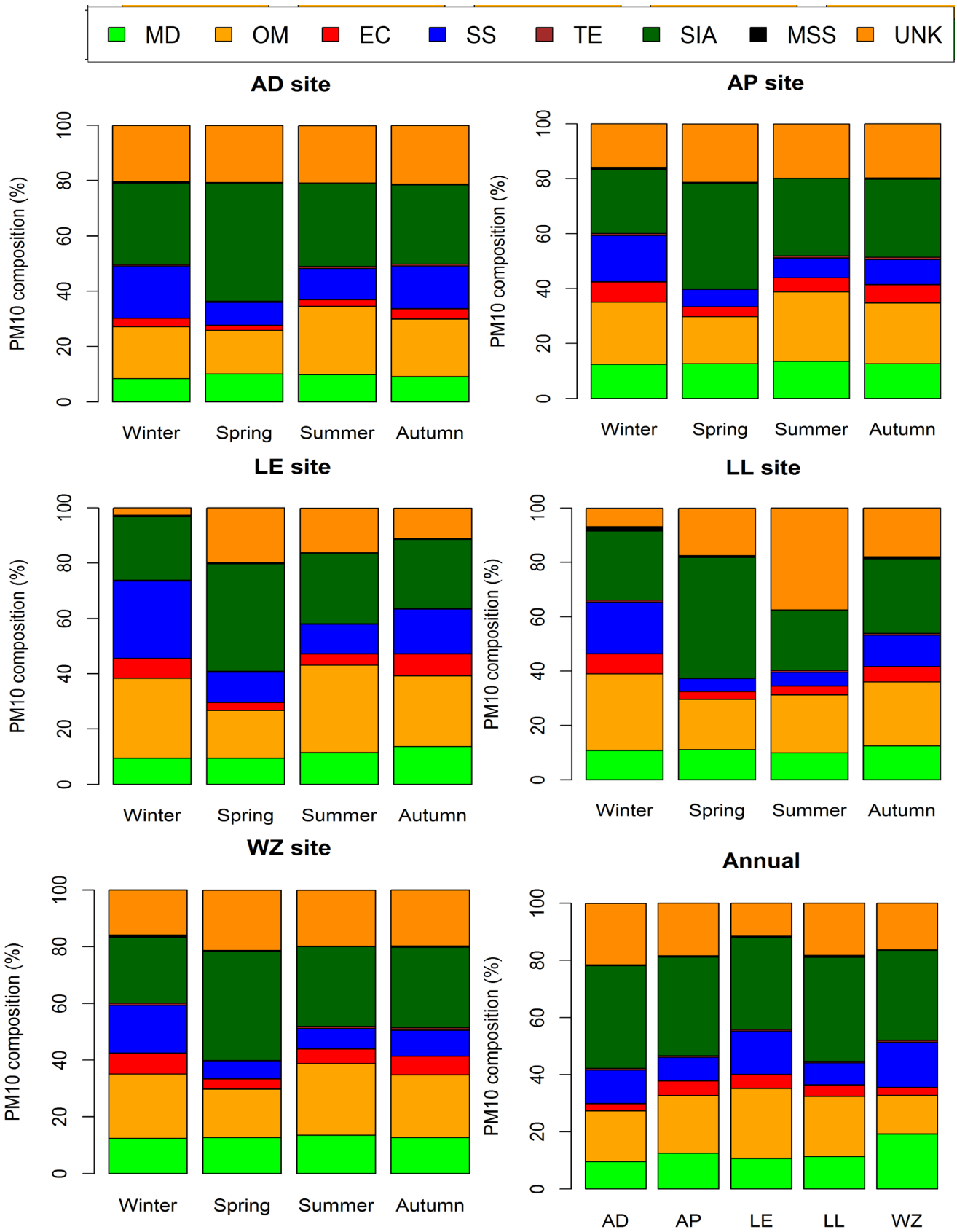Figure 4: Crustal enrichment factor (EF) for the different elements in all cities.

Figure 5: Seasonal and annual chemical mass closure of PM_{10} at five sampling sites.
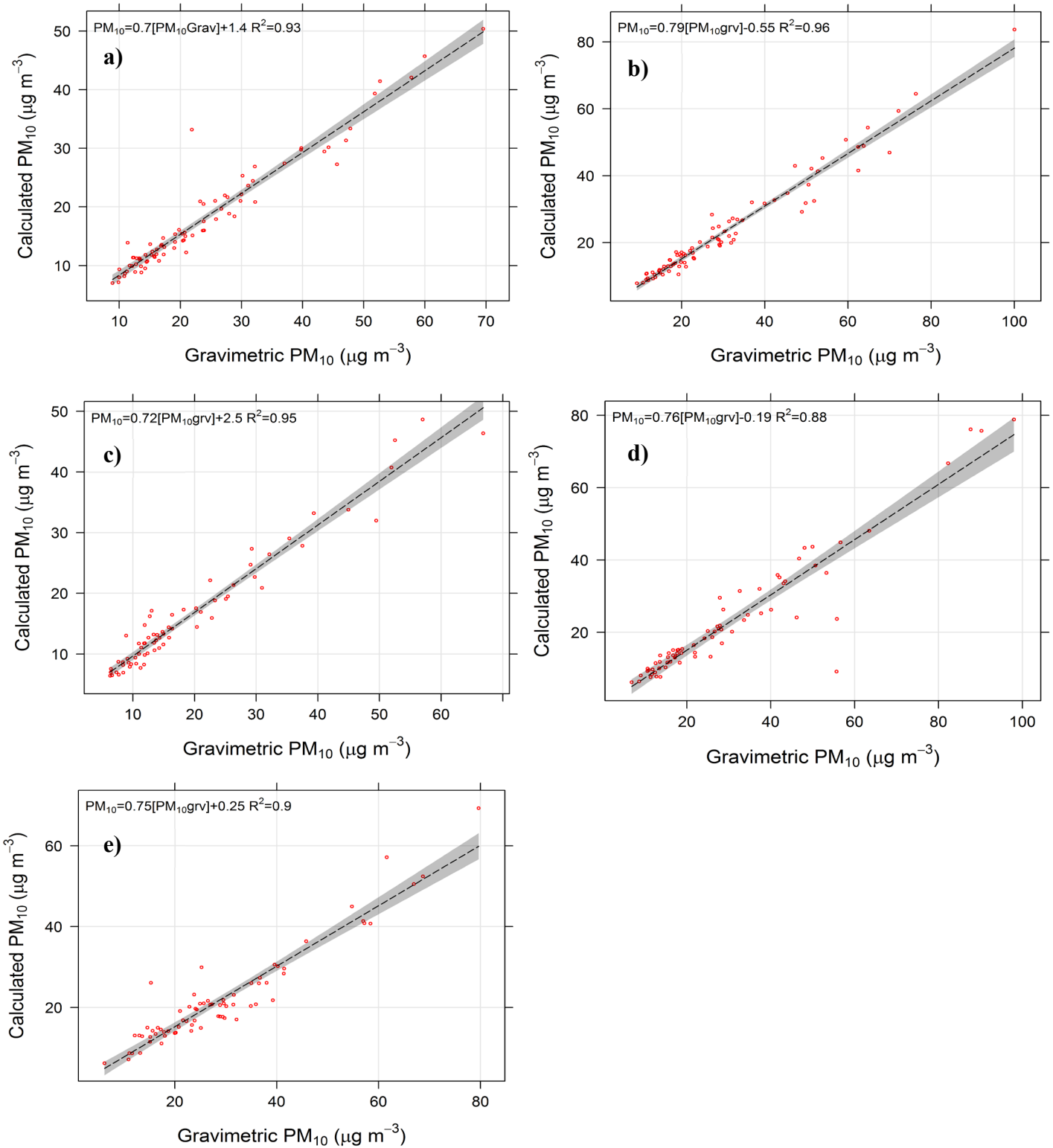
Figure 6: Correlation between the calculated and the gravimetric measured PM_{10} mass concentrations at a) AD, b) AP, c) LE, d) LL, and e) WZ sites.